

DESIGN IMPROVEMENT OF PUMPING MECHANISMS  
IN DAILY NECESSITIES FOR EFFICIENT RECYCLING

by

Sungju Park

APPROVED BY SUPERVISORY COMMITTEE:

---

Wooram Park, Chair

---

Dong Qian

---

Yonas Tadesse

Copyright 2020

Sungju Park

All Rights Reserved

To my parents and Mi Jin Lee

DESIGN IMPROVEMENT OF PUMPING MECHANISMS  
IN DAILY NECESSITIES FOR EFFICIENT RECYCLING

by

SUNGJU PARK, BS

THESIS

Presented to the Faculty of  
The University of Texas at Dallas  
in Partial Fulfillment  
of the Requirements  
for the Degree of

MASTER OF SCIENCE IN  
MECHANICAL ENGINEERING

THE UNIVERSITY OF TEXAS AT DALLAS

December 2020

## ACKNOWLEDGMENTS

I would like to express my sincerest appreciation to my advisor, Dr. Wooram Park, for his guidance, encouragement, and patience throughout my thesis.

I would also like to thank Dr. Yonas Tadesse, and Dr. Dong Qian for serving on my committee.

Finally, I would like to express my deepest thanks to my parents and my wife for their supports and encouragement.

November 2020

DESIGN IMPROVEMENT OF PUMPING MECHANISMS  
IN DAILY NECESSITIES FOR EFFICIENT RECYCLING

Sungju Park, MS  
The University of Texas at Dallas, 2020

Supervising Professor: Wooram Park, Chair

This thesis concerns the design methodology that replaces metallic springs with plastic ones, which will improve the recycling rate of plastic products. Although metallic compression springs are inexpensive and widely used in daily necessities such as sprays and soap pumps, the recycling of the plastic products is highly limited because the non-plastic component is assembled in the products. This limitation should be solved because plastic waste becomes major issue especially in the ocean environment. In this thesis, we propose a design of a stable and effective structure for the plastic spring and perform theoretic analysis to confirm the possibility of practical use of the plastic springs. In addition, the spring models with various design parameters are also analyzed using the finite element method in computer aided design software to calculate spring constants and maximum stresses. The analysis results with various parameters are served as a guideline that can be used to design plastic springs with preferred elasticity. The selected 3D models are 3D-printed for prototyping and the spring constants are experimentally measured for validation of the proposed method.

## TABLE OF CONTENTS

ACKNOWLEDGMENTS .....	v
ABSTRACT.....	vi
LIST OF FIGURES .....	ix
LIST OF TABLES .....	xi
CHAPTER 1 INTRODUCTION .....	1
1.1 Introduction.....	1
1.2 Compliant Mechanism .....	3
CHAPTER 2 THEORETICAL APPROACH.....	5
2.1 Multi-fold structure and base unit.....	5
2.2 Bending of a cantilever beam .....	8
2.3 Bending of an L-shape beam .....	12
2.4 Stiffness estimation of compliant designs.....	15
CHAPTER 3 SIMULATION AND RESULTS.....	18
3.1 Folded spring design .....	20
3.2 Curved spring design .....	25
3.3 Design modification.....	32
3.4 Modification results .....	33
CHAPTER 4 EXPERIMENT AND RESULTS .....	40
4.1 Spring constant test .....	41
4.2 Durability test.....	44
CHAPTER 5 SUMMARY AND FUTURE WORK .....	48
REFERENCES .....	50

BIOGRAPHICAL SKETCH .....	53
CURRICULUM VITAE	



## LIST OF FIGURES

Figure 1. Multi-fold spring structure. ....	5
Figure 2. Half-fold spring structure. ....	6
Figure 3. Free body diagrams for base unit. ....	7
Figure 4. Base unit for stiffness analysis. ....	7
Figure 5. Diagrams of cantilever beam. ....	8
Figure 6. Cantilever beam bending. ....	9
Figure 7. Cantilever beam with moment. ....	11
Figure 8. Separation of the L-shape beam for analysis. ....	12
Figure 9. Base unit bending with angle $\phi_1$ . ....	13
Figure 10. Solidworks model of the first prototype and the final design. ....	19
Figure 11. Half-fold and one-fold structure. ....	20
Figure 12. Solidworks model of 5-folded spring design. ....	21
Figure 13. Maximum stress trend graphs for folded spring models. ....	22
Figure 14. Stress distribution of 0.250 mm thickness, 3.0-folded spring. ....	23
Figure 15. Stress distribution of 0.875 mm thickness, 3.0-folded spring. ....	24
Figure 16. Spring constants trend graphs for folded spring models. ....	25
Figure 17. Half-curve and one-curve. ....	26
Figure 18. Solidworks model of 5-curved spring design. ....	27
Figure 19. Maximum stress trend graphs for curved spring models. ....	28
Figure 20. Stress distribution of 0.500 mm thickness, 2.5-curved spring. ....	29
Figure 21. Stress distribution of 0.500 mm thickness, 3.5-curved spring. ....	29

Figure 22. Stress distribution of 1.250 mm thickness, 3.5-curved spring. ....	30
Figure 23. Spring constant trend graphs for curved spring models. ....	31
Figure 24. Spring design modification.....	33
Figure 25. Spring constant test setup. ....	41
Figure 26. Gram-force of 4.0-fold, 0.750 mm folded spring model with different travel lengths	42
Figure 27. Durability test setup.....	45
Figure 28. Spring compressed in durability test .....	46

## LIST OF TABLES

Table 1. Parameters for 4.0-fold spring structure. ....	15
Table 2. Length $L$ by the thickness of spring structure.....	16
Table 3. Height $a$ by the number of folds. ....	17
Table 4. Theoretical spring constant for folded spring models. ....	17
Table 5. Maximum stress of folded spring design. ....	22
Table 6. Spring constants of folded spring design.....	24
Table 7. Maximum stress of curved spring design. ....	27
Table 8. Spring constants of curved spring design. ....	31
Table 9. Maximum stress of modified folded spring design. ....	34
Table 10. Spring constants of modified folded spring design. ....	34
Table 11. Maximum stress of modified curved spring design.....	35
Table 12. Spring constants of modified curved spring design.....	35
Table 13. Change from modification in percentage.....	36
Table 14. Average change in maximum stress and spring constant by number of folds.....	37
Table 15. Average change in max. stress and spring constant by thickness in folded spring. ....	37
Table 16. Average change in maximum stress and spring constant by number of curves. ....	38
Table 17. Average change in max. stress and spring constant by thickness in curved spring.....	39
Table 18. Spring constants from theory, simulation, and experiment for folded spring design. ....	43
Table 19. Spring constants from theory, simulation, and experiment for curved spring design. ....	43
Table 20. Spring constants before, and after the repetition test for folded spring models. ....	46
Table 21. Spring constants before, and after the repetition test for curved spring models.....	46

# CHAPTER 1

## INTRODUCTION

### 1.1 Introduction

In this world, with 7.8 billion people as of October 2020 [1], waste and landfill become one of the biggest issues. The world generates at least 3.5 million tons of trash a day, and the amount it generates is still increasing rapidly [2]. With a sharp increase in the world population and growth in economies, we are producing more waste than ever.

Plastic is versatile, lightweight, flexible, moisture resistant, strong, and relatively inexpensive material [19]. With its attractive qualities, plastic lead us to voracious appetite and over-consumption of plastic goods, even in vehicle industries [15, 16]. However, durable and very slow to degrade, plastic used for so many products ultimately became waste with staying power [3, 19]. By 2050, A study of the World Economic Forum predicts that there will be so much plastic floating in the ocean so that it will outweigh of fish in the ocean [4]. In 2020, COVID-19 triggered a global use of face masks and gloves and boosted up the growing speed of plastic wastes in the world [28]. The United States is at the top 20<sup>th</sup> in the rank of major sources of plastic debris [5]. On average, a person in the United States uses about 100 kg of plastics every year in which only a small portion is recycled [2]. As the use of plastics for consumer products has become increasingly dominant, and production has steadily increased, the plastic waste is still growing in amount rapidly.

As the usage of plastic becomes broader and wider, recycling of used plastic also becomes important for the environment. In the research of University of Florida [6], plastic

lumber from recycled plastic has high landfill to recycle ratio (LRR), which is the ratio of energy used to land fill a material to the energy used to recycle the material where energy is the energy required to generate a product or service expressed in energy of one form. Higher LRR means that there is more benefit that we can get from recycling. However, according to Ellen MacArthur [7], only 14% of all plastic is collected for recycling after use, and other plastics are just going for landfill. The reason for low recycle rate is from both the unconcern of the people and complexity of some plastic products.

By the British Science Association [8], the top item that people wrongly think that can be recycled is the hand soap pump dispenser tops. A metallic spring in a plastic pump top makes the pump top a multi-compositional package which needs to be separated at the material level to be recycled [9]. In this research, we will improve the design of the pump mechanism in daily necessities like soap dispenser and shampoo head for efficient recycling that does not require separation at material level.

For many daily necessities, pump is attached to a tube which runs into the housing where the liquid is housed. When the pump is pressed by force to activate the pump mechanism, it first pushes air out of the tube to create a suction effect. Then, it draws the liquid back up the tube, releases liquid via the pump spigot. Metallic spring in the pump body enables liquid to pass through the pump mechanism by its elastic motion. In this research, alternative spring to replace the metallic spring is designed and tested to validate the performance. The spring will be designed with plastic for recycling and will be 3D printed for fast prototyping.

Acrylonitrile-Butadiene-Styrene (ABS) plastic has many versatile properties which include thermal resistance, light weight, easy formability, and reflectivity [10]. These properties make

the ABS plastic the most favored material in 3D printing. The elasticity of the material is useful when 3D printing compliant mechanisms such as springs. However, in springs, the geometry of the model interacts with the material properties [11]. That means geometry needs to be changed to achieve certain kinematic behavior with material used in the model. In this research, spring models designed using compliant mechanism with different geometries are tested for its kinematic properties and elastic performance. For pump mechanism in daily necessities, metallic spring is widely used since metallic spring is generally considered as a reliable product. However, pump tops of daily necessities are usually not recycled because of metallic spring since dumping is inexpensive than separating the part to material level and recycle by different material types.

## **1.2 Compliant Mechanism**

The compliant mechanisms are functionally similar to the rigid body mechanisms, but they gain some or all of their mobility from the elastic deflection of flexible members rather than from movable joints only [12, 17, 18]. Traditionally, when designers need a machine that moves, they commonly use very stiff or rigid parts that are connected with hinges or sliding joints [13]. However, over the decades, new materials had been developed, and ability to design more sophisticated devices had been expanded. With the needs from society that cannot be easily addressed using traditional mechanisms, compliant mechanism became more popular with its ability to accomplish complex tasks with fewer parts. There is a potential for increased performance in compliant mechanism over traditional design due to reduced wear and minimized

or eliminated backlash [13]. However, with the advantages, they also have challenges that have to be carefully considered in design. Deflections are often entering into the nonlinear range and simplified linear equations are not adequate to define their motions. Also, because most compliant mechanisms undergo repeated loading, it is important to consider the fatigue life of the device. Design compliant mechanisms with the desired fatigue life can be achieved from understanding of how to achieve controlled compliant mechanism motion and the associated stresses [12]. Despite the difficulties and disadvantages compliant mechanisms have, compliant mechanisms still become more common since they can be compatible with many fabrication methods, may not require assembly, and have friction free and wear free motion. The major challenges associated with compliant mechanisms come from the difficulty associated with design, limited rotation and the need to ensure adequate fatigue life. In this research, we will design spring models performing elastic motion through compliant mechanisms with 3D printer for faster prototyping, using most common 3D printing material ABS [14].

## CHAPTER 2

### THEORETICAL APPROACH

In compliant mechanisms, material achieves force and motion transmission through elastic body deformation. Material gains motion from relative flexibility of its body rather than from rigid joints. Compliant mechanisms rely heavily on the deflection of flexible members, since it stores the energy in those members. Due to their role in compliant mechanism, deflection and elastic behavior of the material are one of the most important factors in the spring model. In this chapter, theoretical approach for bending behavior of elastic material will be reviewed.

#### 2.1 Multi-fold structure and base unit

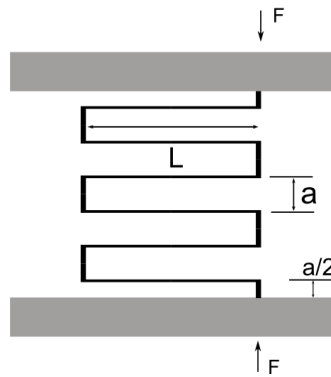


Figure 1. Multi-fold spring structure.

In this chapter, we aim to analyze the elastic behavior of the multi-fold spring structure as shown in Figure 1. The idea of multi-fold spring structure inspired from the leaf springs used in the vehicles. Spiral shape is not the only spring design in the world and we start from flattening



spiral part of the spring to have stair-like shape. In our spring models, two symmetric spring structures with a couple of selected number of folds will be placed between the base plates to perform the elastic behavior. Analyzing multi-fold spring structure starts with splitting the structure to half-fold structure which is the basic structure that serially connected to form the multi-folded structure. Figure 2 shows the structure of half-fold spring.

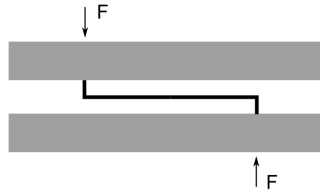


Figure 2. Half-fold spring structure.

When the half-fold spring structure is squeezed, the two ends experience the squeezing force  $F$  as well as the moment  $M$  like a cantilever beam. Due to the symmetry, the same moments should be applied at both ends as it does on Figure 3(a). We can see the same moment  $M$  at each end to cancel each out. For further detailed analysis, we split this half-fold structure at the middle point as shown in Figure 3(b). We should assume there are moments  $M_m$  on the cross sections at the middle point for right and left splits. Figure 3(c) can be obtained by rotating Figure 3(b) by  $360^\circ$ .

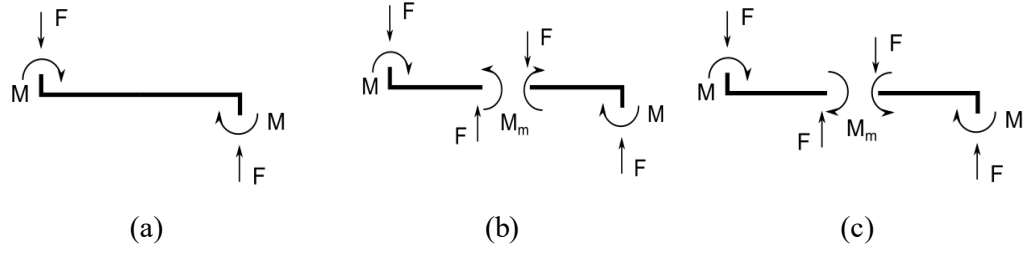


Figure 3. Free body diagrams for base unit.

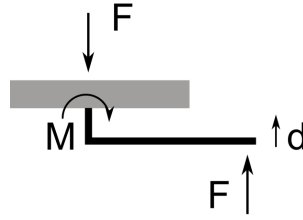


Figure 4. Base unit for stiffness analysis.

By comparing Figure 3(b) and 3(c), we can conclude that the unknown moment  $M_m$  should be zero because the two free body diagrams should be equivalent due to the same geometry, which are external force  $F$  and moment  $M$ . From the fact that  $M_m$  is zero, we can ignore the internal moment and make analysis simpler. Analysis focuses on the left half, separated from half-fold structure with external force  $F$  and moment  $M$  as we can see from Figure 4. As we need to find the stiffness of the system, we can find the stiffness  $k$  with applied force  $F$  and deflection  $d$ .

$$F = k_{stiffness} \times d \quad (2.1)$$

$$k_{stiffness} = \frac{F}{d} \quad (2.2)$$

Analysis on the base unit for stiffness can be further developed by splitting the structure again into a horizontal part and vertical part. From the multi-fold structure, lengths of the vertical beams are  $a$ , and lengths of the horizontal beams are  $\frac{L}{2}$ .

## 2.2 Bending of a cantilever beam

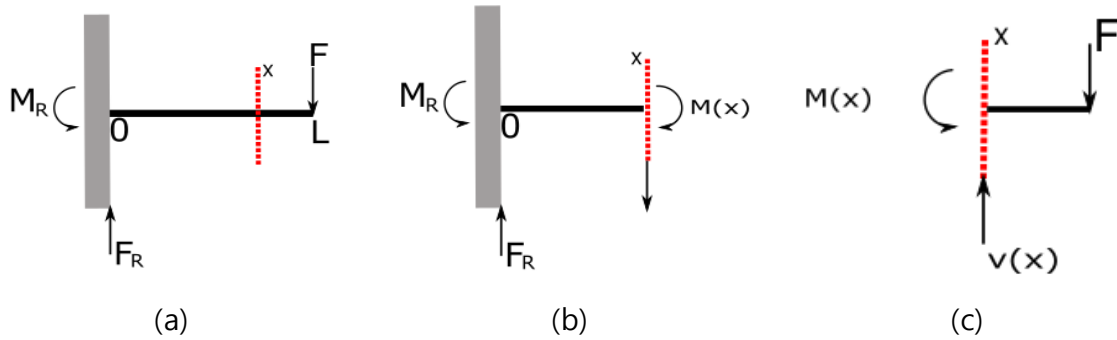


Figure 5. Diagrams of cantilever beam.

Figure 5a shows a cantilever beam with the external force  $F$  and the moment  $M$ . Each segment of the beam must also be in equilibrium. Therefore, it requires that the net force on the object be zero and the total amount of moment about any axis also be zero. As shown in Figure 5(b) and 5(c), equilibrium on each segment of the beam at point  $x$  leads to internal shear force  $V(x)$  and bending moments  $M(x)$ . From Figure 5(c),  $V(x)$  is simply equal to  $F$  and moments  $M(x)$  is calculated as

$$M(x) = -F(L - x). \quad (2.3)$$

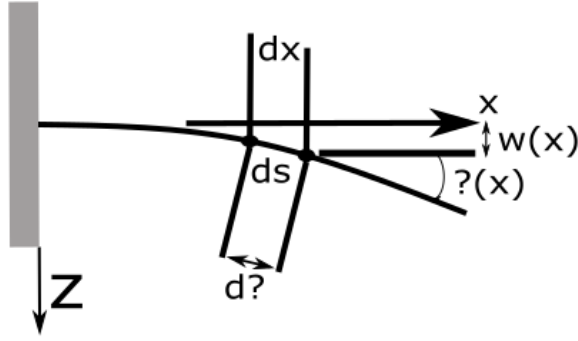


Figure 6. Cantilever beam bending.

Figure 6 shows the bending of the cantilever beam with shape function and angle of the curvature. Deflection of the beam starts from analysis of beam shape function  $w(x)$  as follows [20].

$$\frac{d^2w}{dx^2} = -\frac{M(x)}{EI} \quad (2.4)$$

With relationship of moments  $M(x)$  to external force  $F$  and length in (2.3), the equation (2.4) can be solved by substituting  $M(x)$  by (2.3) and performing integrations with boundary condition of shape function  $w(x)$ , as follows [21].

$$\begin{aligned} \frac{d^2w}{dx^2} &= \frac{F}{EI}(L - x) \\ \frac{dw}{dx} &= -\frac{F}{2EI}x^2 + \frac{FL}{EI}x + A \\ w &= -\frac{F}{6EI}x^3 + \frac{FL}{2EI}x^2 + Ax + B \\ BC: w(0) &= 0, \quad \frac{dw}{dx}\bigg|_{x=0} = 0 \\ A &= B = 0 \end{aligned}$$

$$w = \frac{FL}{2EI}x^2\left(1 - \frac{x}{3L}\right) \quad (2.5)$$

From the shape function from (2.5), the deflection  $d$  at the right end where  $x$  is  $L$  can be derived as

$$d = \frac{FL^3}{3EI}. \quad (2.6)$$

A slope function can be derived from the deflection. If the deflection angle is  $\varphi$ , then the slope is  $\tan(\varphi)$ . However, in the deflection of stiff beam, the deflection and the angle are small enough to linearization. Therefore, the slope can be approximated by the angle  $\varphi$ . Then, the slope shown can be derived by taking derivative of the deflection in (2.5).

$$\varphi = \frac{FL}{2EI} \left( 2x \left( 1 - \frac{x}{3L} \right) + x^2 \left( -\frac{1}{3L} \right) \right) \quad (2.7)$$

At the end of the beam, the slope at  $x=L$  is calculated as

$$\varphi = \frac{FL^2}{2EI}. \quad (2.8)$$

Deflection and slope of the cantilever beam with external force  $F$  have been calculated from (2.1) to (2.8). Deflection and slope, when the external load is only the moment, can be derived in a similar fashion. Figure 7 shows the cantilever beam with moment  $M_o$ .

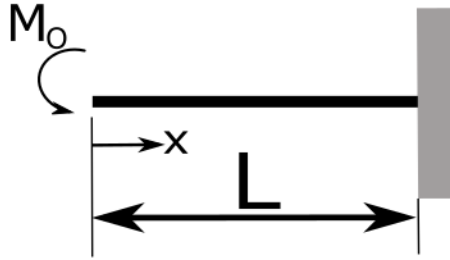


Figure 7. Cantilever beam with moment.

Deflection analysis starts with (2.4). However, the only load is the moment  $M_o$ , so the deflection is derived with same boundary condition for  $w(x)$  as follows.

$$\frac{d^2w}{dx^2} = -\frac{M(x)}{EI}$$

$$M(x) = -M_o$$

$$\frac{d^2w}{dx^2} = \frac{M_o}{EI}$$

$$\frac{dw}{dx} = \frac{M_o}{EI}x + A$$

$$w = \frac{M_o}{2EI}x^2 + Ax + B$$

$$BC: w(0) = 0, \quad \frac{dw}{dx} \Big|_{x=0} = 0$$

$$A = B = 0$$

$$w = \frac{M_o}{2EI}x^2 \tag{2.9}$$

Therefore, from (2.9), the deflection at the end can be derived as

$$d = \frac{M_o L^2}{2EI}. \tag{2.10}$$

As the slope function derived by taking derivative of the deflection for the cantilever beam with external force  $F$ , the slope function for cantilever beam with moment  $M_o$  can also be derived by taking derivative of the deflection in (2.9) as

$$\varphi = \frac{M_o}{EI} x. \quad (2.11)$$

Since the length  $x$  is equal to  $L$  at the end of the beam, the slope at the end of the beam becomes

$$\varphi = \frac{M_o L}{EI}. \quad (2.12)$$

### 2.3 Bending of an L-shape beam

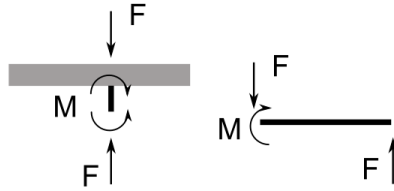


Figure 8. Separation of the L-shape beam for analysis.

The L-shape beam which is the base unit for stiffness analysis is the structure combination of vertical and horizontal beam. It can be analyzed by splitting into two cantilever beams as Figure 8. The L-shape beam has two free body diagrams with one vertical and one horizontal beam with moment  $M$  and force  $F$ . Because the vertical beam has the colinear forces, the lower end should have the moment  $M$  as the other end. This moment  $M$  is also applied at the left end of the horizontal beam for static equilibrium. Therefore, the value of the moment  $M = \frac{FL}{2}$  from the

length of the horizontal beam of  $\frac{L}{2}$ , because the half-fold structure in Figure 2 is cut in half to get the base unit in Figure 4.

In the vertical beam, the deflection due to the compression can be ignored because it is negligible compared to the bending deflection. The deflection for the vertical beam from bending is given as

$$d_0 = \frac{Mx^2}{2EI} = \frac{FLa^2}{16EI}. \quad (2.13)$$

and the bending angle  $\varphi_1$ , using height of  $\frac{a}{2}$  is written as

$$\varphi_1 = \frac{Ma}{EI} = \frac{FLa}{4EI}. \quad (2.14)$$

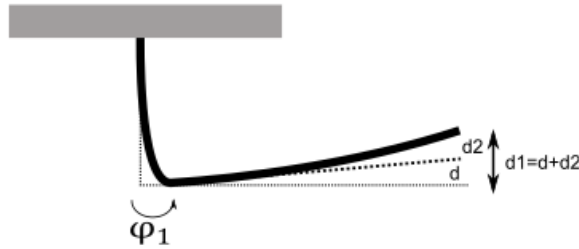


Figure 9. Base unit bending with angle  $\varphi_1$ .

As shown in the Figure 9, due to the angle  $\varphi_1$ , the horizontal bar tilts and right end goes up by  $d$  as

$$d = \varphi_1 \times \frac{L}{2} = \frac{FL^2a}{8EI}. \quad (2.15)$$



In addition to  $d$ , the horizontal beam is deflected due to the force  $F$  and the moment  $M$  shown in the Figure 9. The bending deflection  $d_2$  is calculated using the result in (2.6) from the previous subsection with the length of the beam  $\frac{L}{2}$  instead of  $L$  as

$$d_2 = \frac{F \left(\frac{L}{2}\right)^3}{3EI} = \frac{FL^3}{24EI}. \quad (2.16)$$

Consequently, the total deflection of the structure in Figure 9 is  $d_1$  combining the results from (2.15) and (2.16) as

$$d_1 = d + d_2 = \frac{FL^2 \left(\frac{L}{3} + a\right)}{8EI}. \quad (2.17)$$

Therefore, using the basic stiffness equation (2.2), the stiffness of the base unit  $k_0$  derived as

$$k_0 = \frac{F}{d} = \frac{8EI}{L^2 \left(\frac{L}{3} + a\right)}. \quad (2.18)$$

From the stiffness of the base unit  $k_0$ , we can make the half-fold spring structure in Figure 3 by serially connecting the two base unit structures. A half-fold spring structure has stiffness as

$$k_{half-fold} = \frac{k_0}{2} = \frac{4EI}{L^2 \left(\frac{L}{3} + a\right)}. \quad (2.19)$$

In this manner, the stiffness of a three-folds spring structure in Figure 1 can derived as

$$k_{3-fold} = \frac{k_{half-fold}}{2N} = \frac{k_0}{12} = \frac{2EI}{3L^2 \left(\frac{L}{3} + a\right)}. \quad (2.20)$$

since the structure can be made by serially connecting 12 base units or 6 half-fold units.

## 2.4 Stiffness estimation of compliant designs

In this subsection, we perform the estimation of the compliant structures that we are considering in this research. In 2.3, we derived the spring constant of the base unit which is the half of the half fold spring structure as in (2.18). Using the equation (2.18), and properties of the spring structure including elastic modulus  $E$ , moment of inertia  $I$ , horizontal length of the beam  $L$  and vertical height  $a$  of the spring which is the gap between horizontal beams, the spring constant for each spring structures in this research can be calculated. Universal variables for the spring models are the Young's modulus  $E$ , which is 2000N/mm<sup>2</sup> from Material Properties of ABS [23] and also from ABS plastic material properties we used in Solidworks for simulation section.

For instance, we calculate the spring constant of modified 4.0-fold spring model with 0.500 mm thickness. The parameters for the calculation are shown in Table 1. The moment of inertia  $I$  for a rectangular section is calculated through the equation

$$I = \frac{bh^3}{12} \quad (2.21)$$

where  $b$  is the length and  $h$  are the height of the rectangular cross section [22].

Table 1. Parameters for 4.0-fold spring structure.

Structure	$E$	$I$	$L$	$a$
4.0	2000.0	0.1458	9.75	3.38

Example model with thickness of 0.500 mm and 4.0-fold spring structure is composed of 8 half fold units which is again, composed of 16 base units. The spring constant of this spring structure is

$$k_{4.0-fold} = \frac{k_{half-fold}}{8} = \frac{k_0}{16} = \frac{EI}{2L^2 \left( \frac{L}{3} + a \right)} = 0.2315 \text{ N/mm}. \quad (2.22)$$

Since our spring model has two spring structures in parallel between the top and bottom plates, the spring constant of the whole model can be obtained by doubling the spring constant of a single-spring structure. Therefore, the spring constant for the whole spring structure is calculates as

$$k_{model} = 2 \times k_{4.0-fold} = 0.4631 \text{ N/mm}. \quad (2.23)$$

For the spring models in this research, the length  $L$  depends on the thickness because the starting point of the vertical beam is fixed, and the length  $L$  needs to be changed to have the exact gap of 2 mm between the spring structures after design modification of Chapter 3.3. The height  $a$  depends on the number of fold structure. All spring models with different number of folds share equal total height from top plate to bottom plate with equal thickness of two plates. Consequently, when the fold number increases, the height of the fold decreases. Tables 2 and 3 summarizes the length  $L$  by the thickness and the height  $a$  by the number of folds.

Table 2. Length  $L$  by the thickness of spring structure.

Thickness	0.250	0.375	0.500	0.625	0.750	0.875	1.000	1.125	1.250	1.500
$L$ (mm)	9.875	9.815	9.750	9.690	9.625	9.565	9.500	9.440	9.375	9.250

Table 3. Height  $a$  by the number of folds.

Fold Number	1.0	1.5	2.0	2.5	3.0	3.5	4.0	4.5	5.0
$a$ (mm)	13.500	9.000	6.750	5.400	4.500	3.857	3.375	3.000	2.700

With the variables, and equation (2.18), spring constant for each spring models with thickness varying from 0.250 mm to 1.500 mm and the numbers of folds varying from 1 to 5 are shown in the Table 4.

Table 4. Theoretical spring constant for folded spring models.

Spring Constant (N/mm)										
Thickness # of Fold	0.250	0.375	0.500	0.625	0.750	0.875	1.000	1.125	1.250	1.500
1	0.0891	0.3046	0.7327	1.4506	2.5438	4.0952	6.2050	8.9582	12.4756	22.2001
1.5	0.0811	0.2776	0.6679	1.3229	2.3210	3.7381	5.6667	8.1847	11.4038	20.3118
2	0.0745	0.2549	0.6136	1.2158	2.1340	3.4383	5.2143	7.5341	10.5016	18.7196
2.5	0.0688	0.2357	0.5675	1.1248	1.9750	3.1830	4.8288	6.9793	9.7317	17.3588
3	0.0640	0.2191	0.5279	1.0465	1.8380	2.9630	4.4964	6.5007	9.0670	16.1825
3.5	0.0598	0.2048	0.4934	0.9784	1.7188	2.7715	4.2069	6.0835	8.4874	15.1558
4	0.0561	0.1922	0.4631	0.9185	1.6140	2.6032	3.9522	5.7165	7.9772	14.2510
4.5	0.0528	0.1810	0.4364	0.8656	1.5214	2.4542	3.7267	5.3914	7.5250	13.4485
5	0.0499	0.1711	0.4125	0.8185	1.4387	2.3213	3.5256	5.1012	7.1213	12.7315

From the Table 4, we can conclude that the spring constant increases as the thickness increases, but decreases when the fold number increases with the fixed thickness. This was expected in the equation (2.18). The moment of inertia  $I$  is directly proportional to the thickness, and the spring constant is inversely proportional to the number of folds since the base unit is serially connected [24].

## **CHAPTER 3**

### **SIMULATION AND RESULTS**

It is not always possible for analytical models to completely describe the performance of a whole mechanism. Therefore, mechanisms are often analyzed using finite-element models in simulating software. Models created in the CAD is going under structural analysis that uses finite element analysis (FEA) to predict models' real-world physical behaviors. Simulation of the models testifies the analytical idea that we developed in Chapter 2, and analysis of the result optimizes the spring design. In this chapter, spring models are developed in 3D CAD application to perform simulation of elastic behavior and FEA.

In modeling the plastic springs, a key to obtain stable and effective structure is the design methodology. For the basic objective of replacing the springs in daily necessities such as shampoo dispenser, dimensions of the spring should be determined by the size of the dispenser. From the sample shampoo dispenser mechanism model, we obtain the spring height of 31 mm. The difference of material properties of the ABS plastic and carbon steel or stainless steel, normally used in metallic spring leads to difference in spring structure. Since, Young's modulus of plastic and steel are very different, the diameter of the spring needed to be increased up to the point where it does not have interference with the pump model. Compared to the diameter of 10 mm in metallic spring of a mechanism model of a sample shampoo dispenser, the maximum diameter of the spring without the interference is used in the spring design which is 28 mm. First prototypes had been built with top, and bottom plate of 1mm thickness, and tested. Due to low stress limit from the thickness, one prototype had crack at the plate. Final designs of the plastic

springs have top, and bottom plate of 2 mm thickness and 27 mm height of spring structure in between.

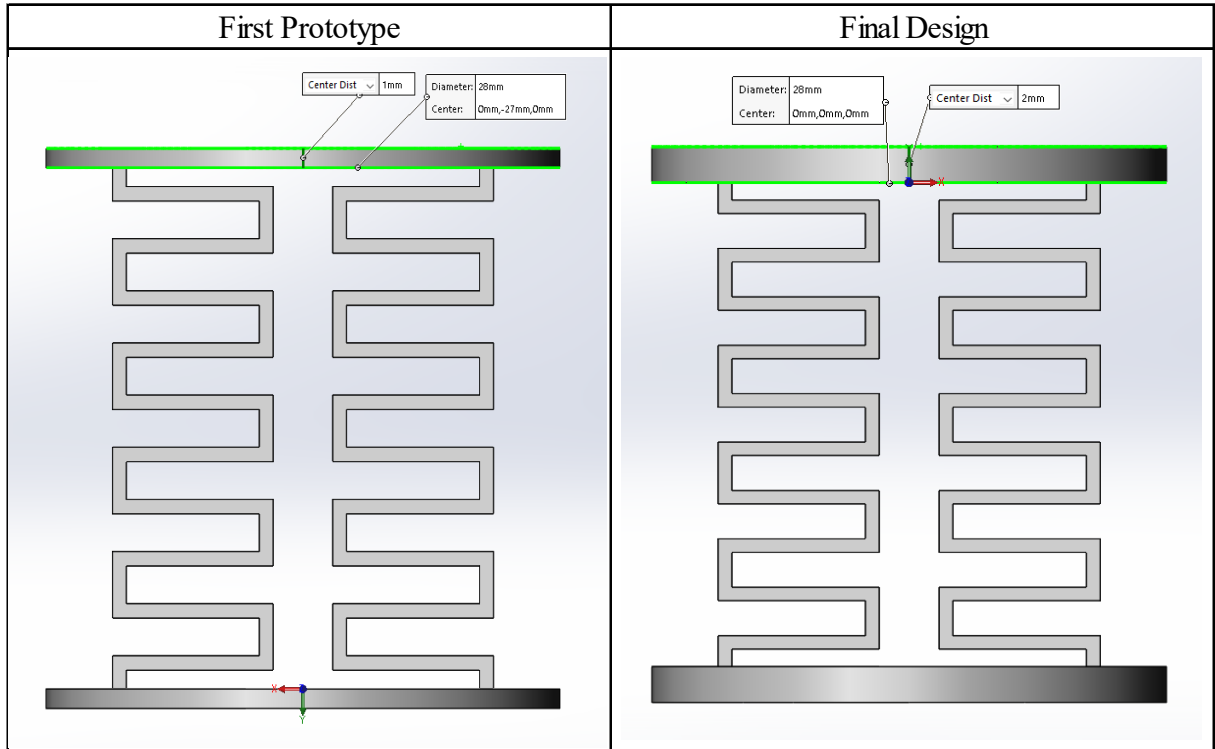


Figure 10. Solidworks model of the first prototype and the final design.

In this chapter, we present a method for determining the spring constant and analyzing the maximum stress in the models to optimize the design variables in the plastic springs. The pump mechanism in shampoo dispensers has housing and spring seat to mount the spring constraints in distortion but only allows the compression of the spring. Our basic assumption is that the springs with bottom fixed to ground, will experience the displacement in direction of compression, but do not experience any other displacements. In this chapter, plastic spring

models with thickness and number of spring structures as design variables, with fixed compression displacement are simulated for optimization of the spring design. Finite element analysis is carried out using CAD software, Solidworks 2019.

### 3.1 Folded spring design

The L-shape beam deflection from Chapter 2 is used to design folded spring model. By combining two L-shape structure, which was defined as a base unit, we can make a half-fold structure as Figure 11. Likewise, a one-fold structure is made with two identical half folds as shown in Figure 11.

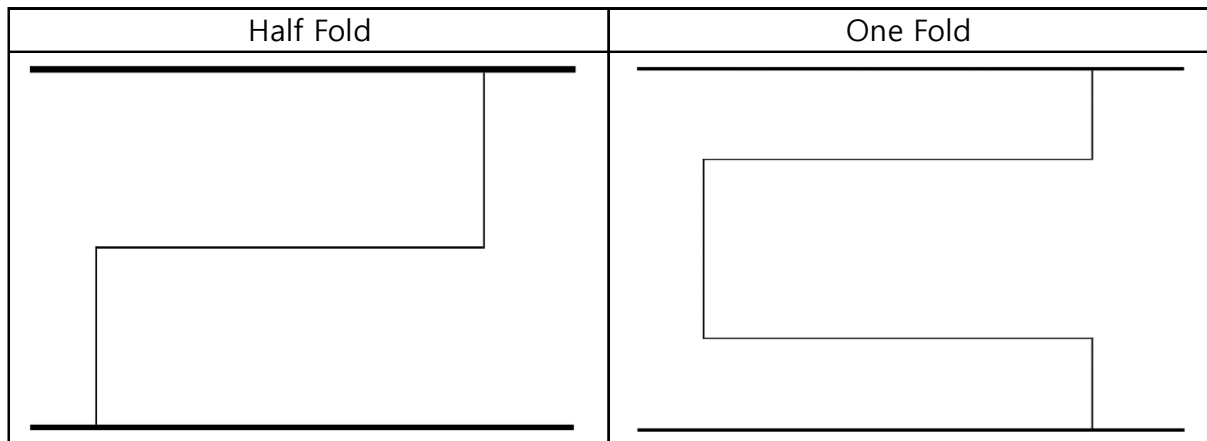


Figure 11. Half-fold and one-fold structure.

The folded spring model is constructed with the top and bottom plates with 1mm thickness and symmetrical spring structures between the plates composed of one-fold to five-folds with increment of half-fold. After profile of spring structure is sketched from the top plate,

the thickness of the spring is constructed by offsetting the profile by half of thickness to both directions.

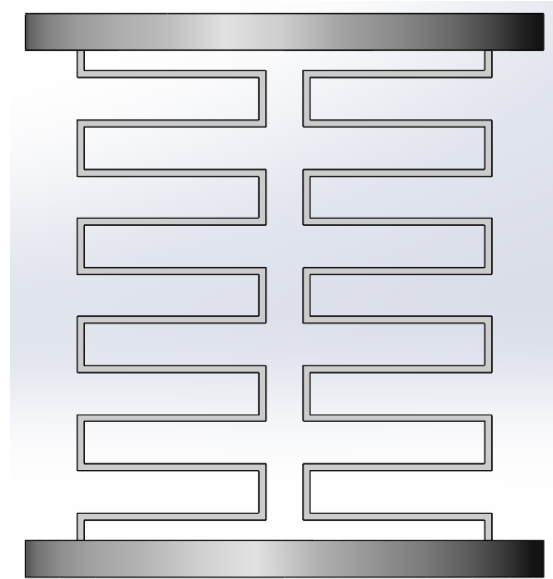


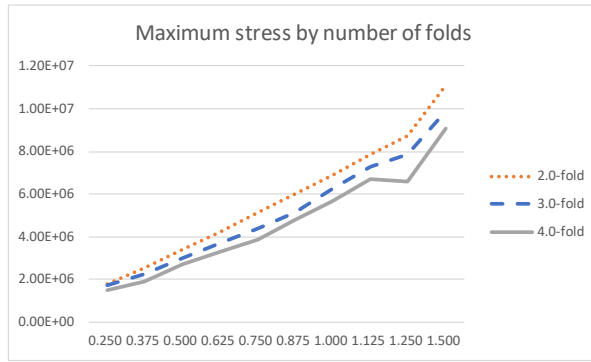
Figure 12. Solidworks model of 5-folded spring design.

The constructed model then goes through the static simulation with x, and y displacement of 0 mm to remove any distortion or shear but z direction of -1 mm to analyze the distribution of the stress and force needed for distance of 1 mm to spring to determine the spring constant. The maximum stress results are shown in Table 5 with Young's modulus of  $2000\text{N/mm}^2$  from Solidworks' material selection as mentioned previously in Chapter 2.

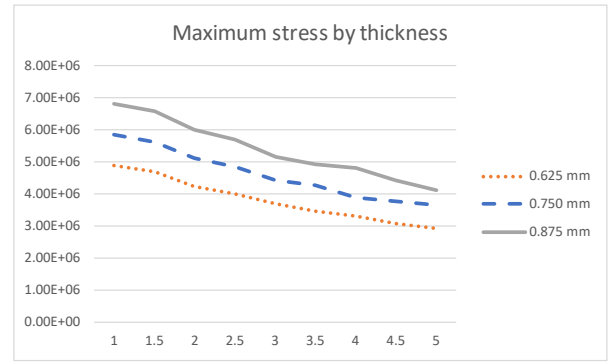


Table 5. Maximum stress of folded spring design.

Maximum Stress (N/m <sup>2</sup> ) - 1mm movement										
Thickness # of Fold	0.250	0.375	0.500	0.625	0.750	0.875	1.000	1.125	1.250	1.500
1	2.47E+06	3.74E+06	5.39E+06	6.12E+06	7.30E+06	8.50E+06	9.77E+06	1.10E+07	1.21E+07	1.45E+07
1.5	2.57E+06	3.67E+06	4.83E+06	5.98E+06	7.06E+06	8.25E+06	9.41E+06	1.07E+07	1.20E+07	1.44E+07
2	2.31E+06	3.32E+06	4.39E+06	5.42E+06	6.49E+06	7.52E+06	8.63E+06	9.67E+06	1.08E+07	1.31E+07
2.5	2.23E+06	3.27E+06	4.22E+06	5.23E+06	6.24E+06	7.28E+06	8.44E+06	9.42E+06	1.07E+07	1.28E+07
3	2.26E+06	3.24E+06	3.94E+06	4.85E+06	5.72E+06	6.75E+06	7.79E+06	9.18E+06	9.92E+06	1.21E+07
3.5	2.14E+06	2.84E+06	3.72E+06	4.62E+06	5.51E+06	6.43E+06	7.72E+06	9.13E+06	9.66E+06	1.18E+07
4	2.05E+06	2.66E+06	3.73E+06	4.44E+06	5.28E+06	6.32E+06	7.42E+06	8.69E+06	8.48E+06	1.12E+07
4.5	1.97E+06	2.69E+06	3.21E+06	4.14E+06	5.17E+06	5.78E+06	6.57E+06	7.51E+06	8.51E+06	1.11E+07
5	1.86E+06	2.56E+06	3.25E+06	3.96E+06	4.77E+06	5.42E+06	6.31E+06	7.11E+06	8.34E+06	1.13E+07



(a)



(b)

Figure 13. Maximum stress trend graphs for folded spring models.

The maximum stress has a basic trend of increasing as the thickness increase since the force needed to move the spring 1 mm down increases as the thickness increases. As the fold number increases, the stress gets distributed and we get the results of getting decreased in most of the cases. As in Figure 14, 0.25 mm thickness models show that the maximum stress is exerted at the horizontal edge of the fold due to their low thickness profile. This phenomenon only occurs at springs with 0.25 mm thickness. For other thicknesses, the maximum stress can be

found at inside or outside the vertical beam of the spring. And as in Figure 15, the stress distributed intensively at vertical beams of the fold due to spring's vertical displacement. The area of the intensive stress at the outer surface of the vertical beam has height of inner surface inside the fold. In the inner surface the intensive stress has been exerted for smaller area than inner surface. As the fold number increases and thickness increases, the stress in inner surface form a line in the middle of the inner wall.

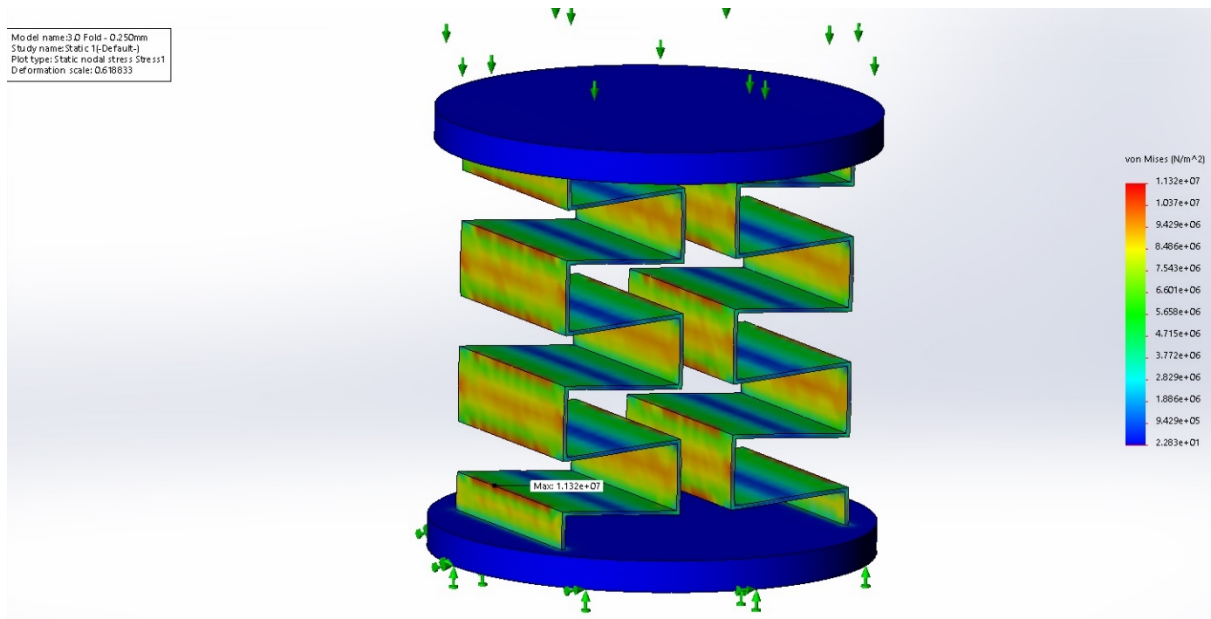


Figure 14. Stress distribution of 0.250 mm thickness, 3.0-folded spring.

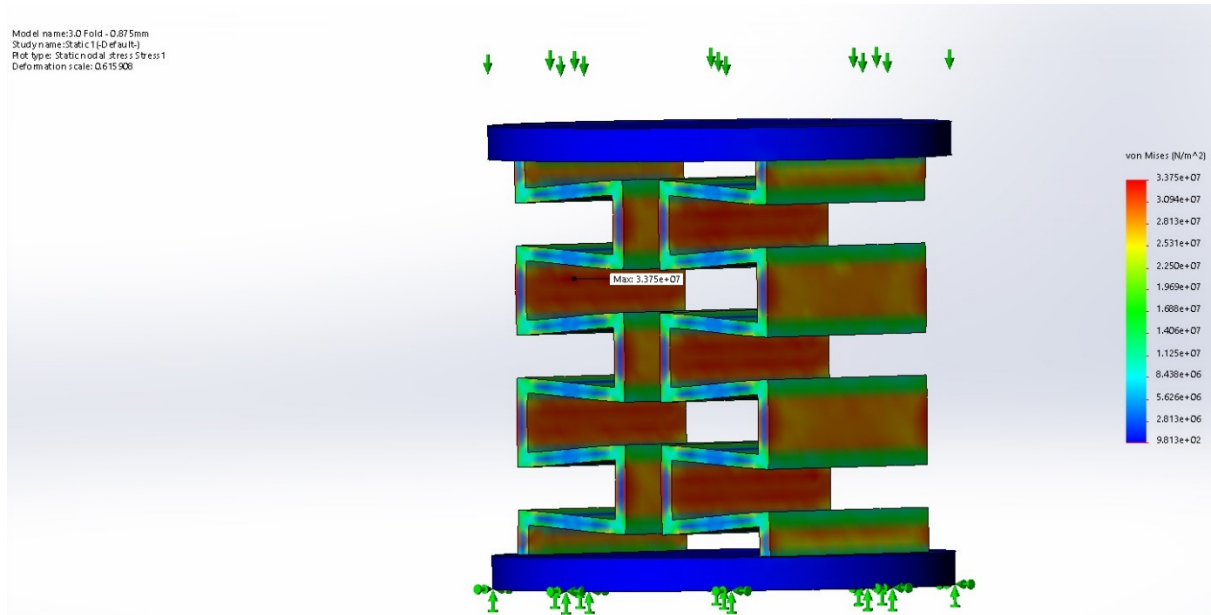


Figure 15. Stress distribution of 0.875 mm thickness, 3.0-folded spring.

A spring constant is representing how stiff the spring is, which means how much force is needed to move the spring. The spring constants of the plastic spring models get calculated from the force needed to move the spring models 1 mm downward from simulations using Hooke's Law. Table 6 shows the resulting spring constants.

Table 6. Spring constants of folded spring design

Spring Costant (N/mm)										
Thickness # of Fold	0.250	0.375	0.500	0.625	0.750	0.875	1.000	1.125	1.250	1.500
1	0.18238	0.59967	1.3876	2.6684	4.5916	7.2418	10.779	15.339	20.816	35.515
1.5	0.17952	0.5851	1.3456	2.578	4.4056	6.9611	10.355	14.794	20.097	34.452
2	0.17336	0.56889	1.2851	2.4553	4.1939	6.6236	9.899	14.124	19.009	32.877
2.5	0.16694	0.54501	1.243	2.3682	4.0342	6.3768	9.5224	13.61	18.295	31.681
3	0.16436	0.53041	1.1727	2.2324	3.8105	6.0365	9.0884	13.065	17.753	30.548
3.5	0.15789	0.51563	1.1427	2.1694	3.6943	5.8548	8.7802	12.618	16.703	29.186
4	0.15149	0.48486	1.0963	2.0811	3.539	5.6011	8.3435	12.01	16.555	28.448
4.5	0.1512	0.48603	1.0928	1.9675	3.3633	5.368	8.0762	11.714	15.951	27.195
5	0.14509	0.46119	1.0376	1.9709	3.3474	5.1284	7.7523	11.265	14.943	26.161

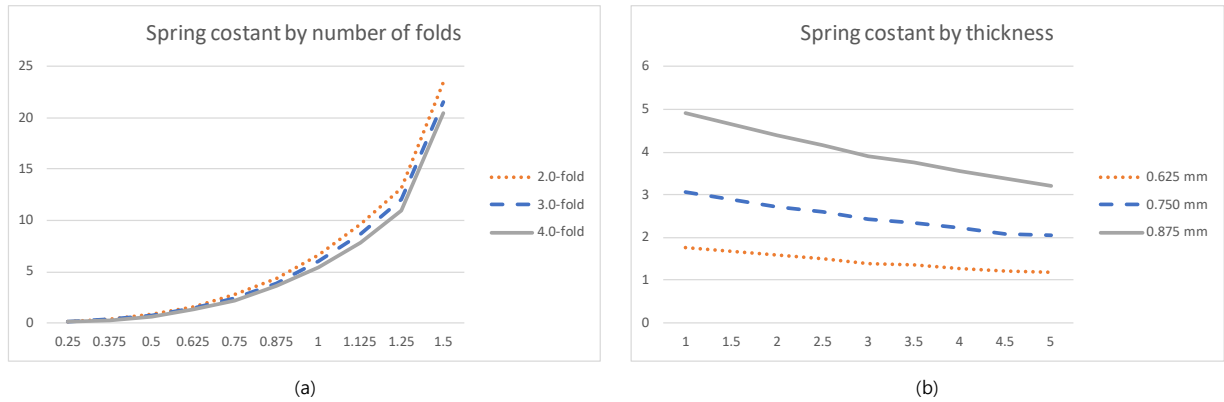


Figure 16. Spring constants trend graphs for folded spring models.

As the trend of the maximum stress in the spring does, the spring constant also increases as the thickness increases and decreases as the fold number increases. If one needs to select the spring model for specific application, model selection can be started from defining the spring constant range depending on the application then, create a list of applicable spring models with different parameters from Table 6.

### 3.2 Curved spring design

A curved spring model is designed as an alternative model after observing intensive stress concentration in the vertical beam of the folded spring model above. In designing the model, basic assumption has been made that stress will be distributed more uniformly as the edges are round. The half curve is made by replacing the edge of the half hold with circular arc with the diameter equal to the height. The one curve is constructed by combining two half curves as shown in Figure 17.

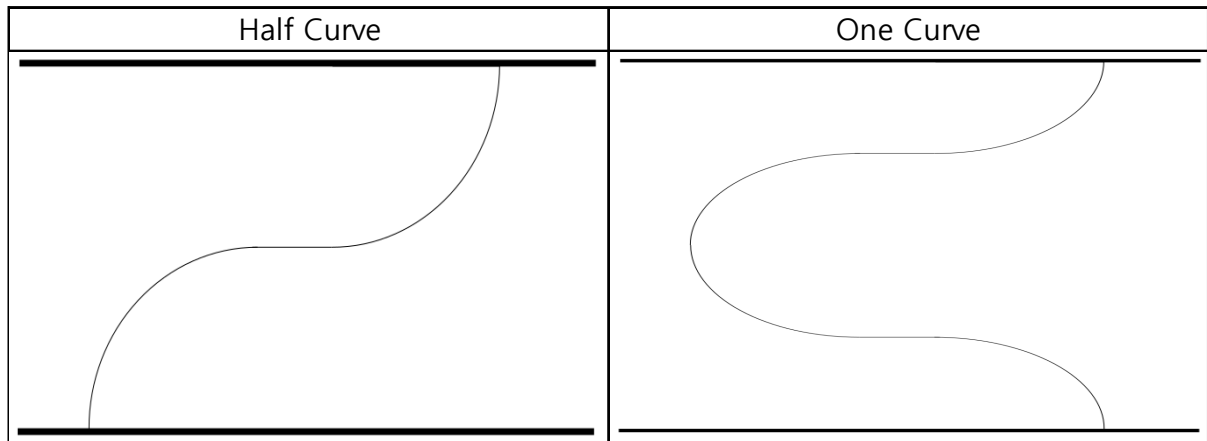


Figure 17. Half-curve and one-curve.

With the same dimensions as in the folded spring model with the top and bottom plates, the folded spring design is modified to have curves instead of folds. For the curved spring model, the 3D model is constructed by modifying the folded spring model. Two different fillets have been applied to maintain the thickness through the spring structure. Smaller fillet with radius of half the diameter subtracted by half the thickness has been applied at interior edges while, larger fillet with radius of half the diameter added by half the thickness has been applied at exterior edges so that the curve has the right thickness. For the one folded spring models, which has the biggest height, curve profile is not applicable since fillets overlapped each other from the big fillet radius. The one-curve model is disregarded since the thickness is not obtained equally throughout the spring structure. With the symmetric spring structures between plates, the models are made with one and a half-curve to five-curves with increment of half-curve.

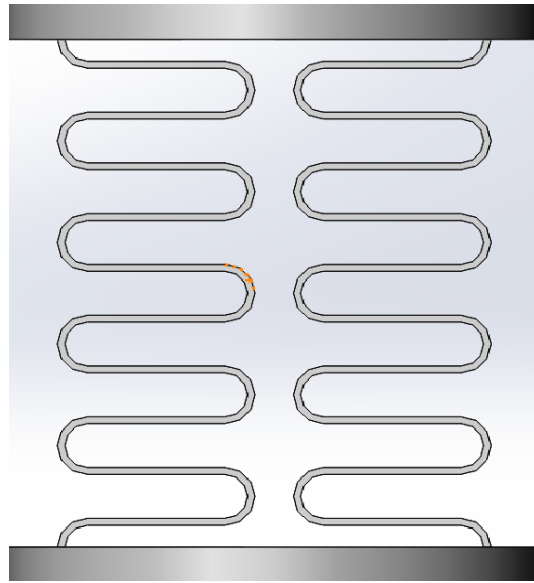


Figure 18. Solidworks model of 5-curved spring design.

The curved spring models then go through the static simulation set equally to that of folded spring models with x, and y displacement of 0 mm to remove any distortion or shear but z direction of -1 mm to analyze the distribution of the stress and force needed for distance of 1 mm to spring to determine the spring constant. The resulting maximum stresses are shown in Table 7.

Table 7. Maximum stress of curved spring design.

Maximum Stress (N/m <sup>2</sup> ) - 1mm movement										
Thickness # of Curve	0.25	0.375	0.5	0.625	0.75	0.875	1	1.125	1.25	1.5
1										
1.5	7.02E+06	7.35E+06	1.12E+07	1.28E+07	1.42E+07	1.56E+07	1.65E+07	1.77E+07	2.05E+07	2.48E+07
2	5.20E+06	5.54E+06	7.08E+06	8.24E+06	9.49E+06	1.08E+07	1.23E+07	1.39E+07	1.69E+07	1.97E+07
2.5	4.89E+06	6.30E+06	6.67E+06	8.11E+06	8.86E+06	1.06E+07	1.13E+07	1.28E+07	1.44E+07	1.90E+07
3	5.02E+06	5.20E+06	5.98E+06	7.32E+06	7.95E+06	8.87E+06	1.01E+07	1.14E+07	1.35E+07	1.70E+07
3.5	5.10E+06	6.28E+06	8.00E+06	7.20E+06	7.22E+06	8.17E+06	1.08E+07	1.09E+07	1.35E+07	1.81E+07
4	3.17E+06	4.69E+06	5.91E+06	7.25E+06	7.05E+06	8.07E+06	9.19E+06	9.23E+06	1.33E+07	1.66E+07
4.5	2.86E+06	5.31E+06	5.37E+06	5.77E+06	5.90E+06	6.22E+06	9.37E+06	9.20E+06	1.17E+07	1.40E+07
5	3.04E+06	4.11E+06	5.02E+06	5.10E+06	6.05E+06	6.84E+06	7.96E+06	8.82E+06	1.07E+07	1.43E+07

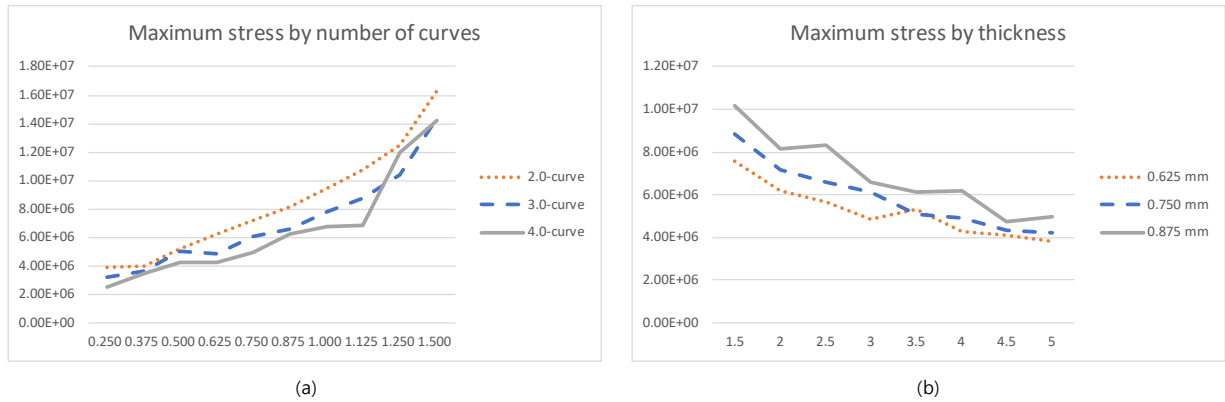


Figure 19. Maximum stress trend graphs for curved spring models.

The basic trend for the maximum stress is equal to that of the folded spring models. The maximum stress increases as the thickness increases since the force needed to move the spring equal distance down increases. The number of curves has impact on the stress by distributing the stress to more curves and decreases the maximum stress when they are tested with the equal thickness. In the low thickness, or low number of curves, the maximum stresses occur at the edge or exterior surface of the curve randomly as in Figure 20. However, over 3.5 curves, and over .5 mm thickness, every curved spring model have their maximum stress at interior surface of the curve feature as in Figure 21.

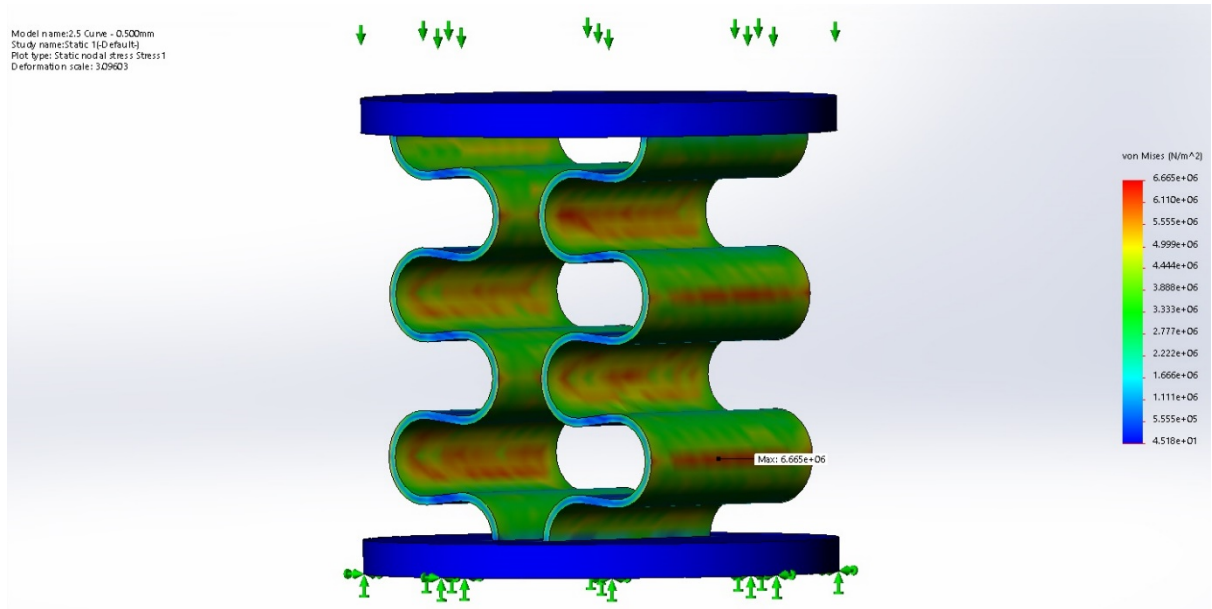


Figure 20. Stress distribution of 0.500 mm thickness, 2.5-curved spring.

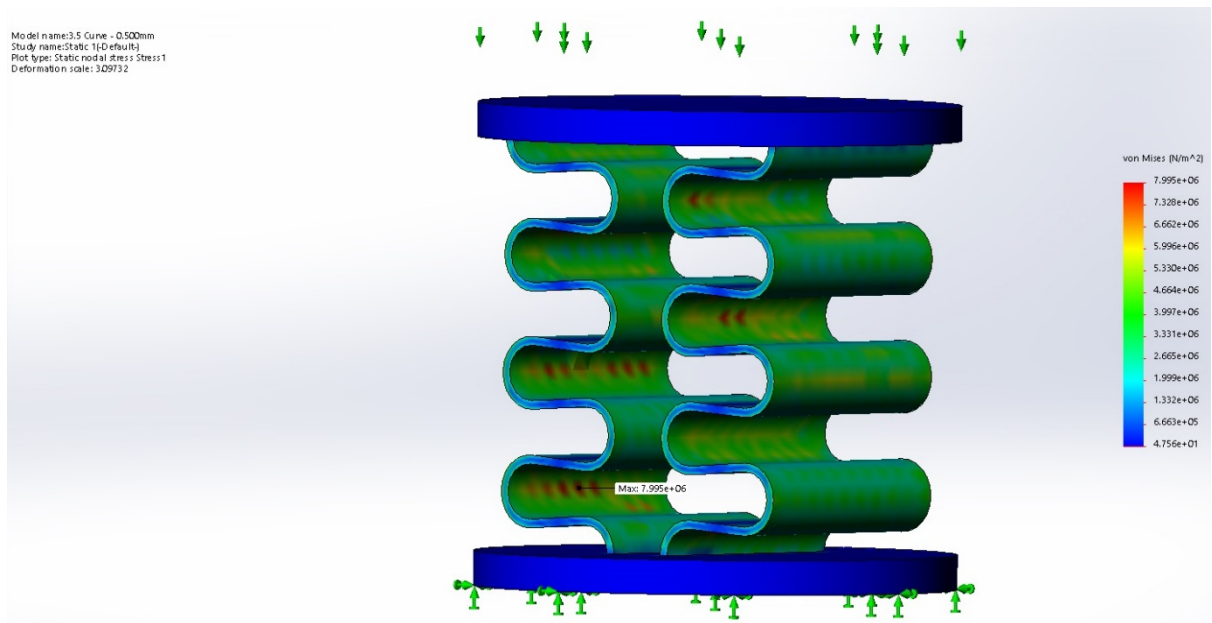


Figure 21. Stress distribution of 0.500 mm thickness, 3.5-curved spring.



In the models with thickness over 0.5 mm, as the thickness increases, the stresses are concentrated at the interior surface, and the exterior surface of the curve experience the lower stress compared to the interior surface as the thickness increases. That means, in the very thick models, including 1.25 mm and 1.5 mm, the areas with high stress do not exist at the outer surface of curves. However, the stress is intensively distributed at the interior surface of the curve where it folds.

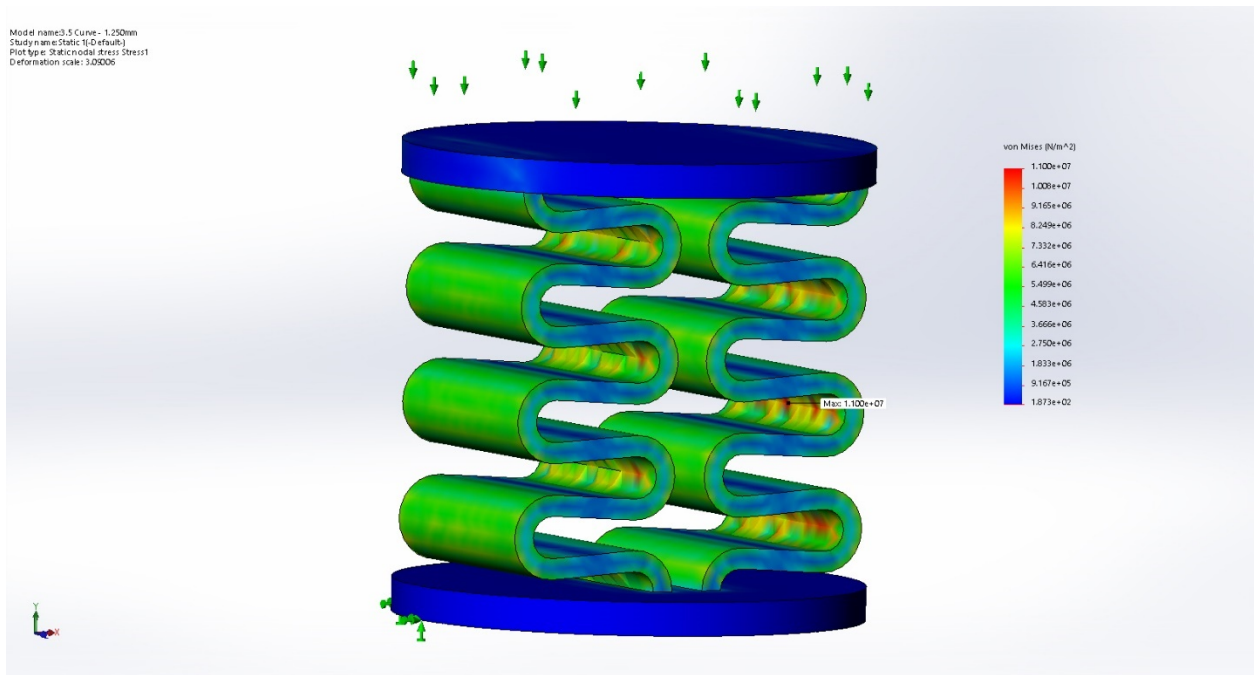


Figure 22. Stress distribution of 1.250 mm thickness, 3.5-curved spring.

As in the folded spring model, the spring constant is calculated from the force needed to press the spring – 1 mm in z direction. Table 8 shows the results of the spring constants.

Table 8. Spring constants of curved spring design.

Thickness # of Curve	0.25	0.375	0.5	0.625	0.75	0.875	1	1.125	1.25	1.5
1										
1.5	0.42698	1.1284	2.4672	4.612	7.7541	12.075	17.749	24.957	33.784	56.551
2	0.30938	0.84161	1.9172	3.6032	6.1292	9.6609	14.352	20.364	27.905	46.628
2.5	0.34262	0.8003	1.6988	3.206	5.4771	8.6889	12.764	18.128	24.828	41.686
3	0.41833	0.78915	1.5742	2.9271	4.9676	7.8456	11.697	16.593	22.784	37.759
3.5	0.38189	0.84383	1.5566	2.7457	4.5188	7.178	10.725	15.304	24.173	36.839
4	0.30635	0.68928	1.3184	2.4713	4.7522	6.9994	10.111	14.376	19.997	32.555
4.5	0.24768	1.1786	1.7419	2.6467	4.1183	6.2891	9.3364	13.32	18.343	31.951
5	0.36982	0.88293	1.4068	2.2956	3.7307	5.8513	8.7967	12.476	17.281	28.065

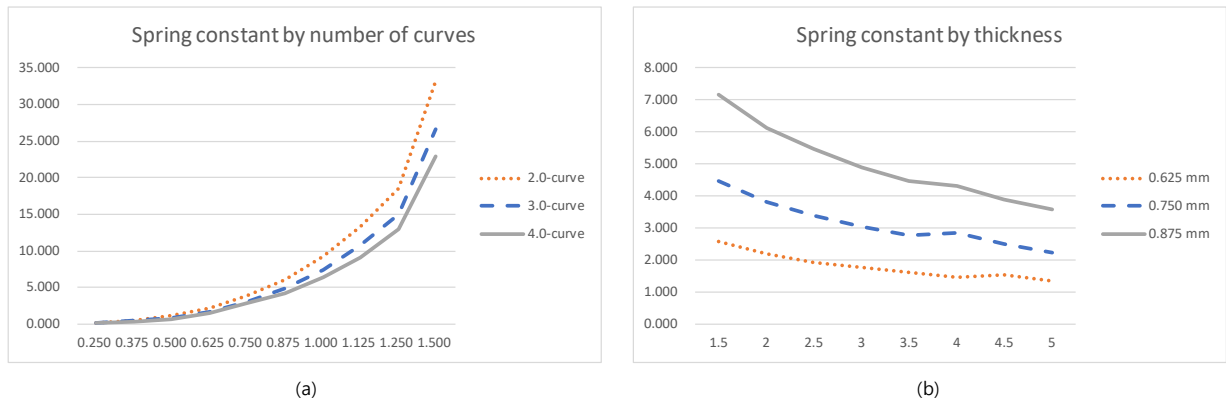


Figure 23. Spring constant trend graphs for curved spring models.

As the trend of spring constants of the folded spring model does, in the curved spring model, the spring constant increases as the thickness increases and decreases as the fold number increases. The amount of spring constant decrease gets larger as the thickness increases where at the 1.5 mm thickness, the spring constant decreases by about 50% from one and a half curve to 5 curves. With the table, the list of applicable spring models can be obtained from the targeted range of spring constant for application. The list contains different thicknesses and numbers of

curves compared to the folded spring model's list since the spring constant is different for the same thickness and number of curve or fold.

### **3.3 Design modification**

The spring model needs to have lower spring stiffness with the same thickness in order to be more flexible to experience lower stress when compressed to the same distance. The folded and curved spring models in Chapter 3 need improved spring constants so that the models have lower stiffness with the same thickness. The folded and curved spring models originate their design in the beam deflection theory. In the beam deflection theory, the maximum deflection and stiffness value were impacted by the beam length. In order to increase the maximum deflection and decrease the stiffness, the beam length needs to be increased.

The spring models used in the previous simulations have symmetric structures by the center line with a gap between them. In order to extend the length, two modifications have been made to all models. The first modification is made at the distance between the starting point of the spring structure to the centerline. The distance is increased by 1 mm which means the spring structures moved back toward out by 1 mm. The second modification is made at the distance between the two spring structures. For all folded and curved spring models, a gap between the spring structures have been fixed to 2 mm in order to have the minimum gap which ensures no interference between the structures. Minimizing the gap between the spring structures is connected to maximizing the length of the beam part of the spring structure to lower the spring stiffness with the same spring thickness.

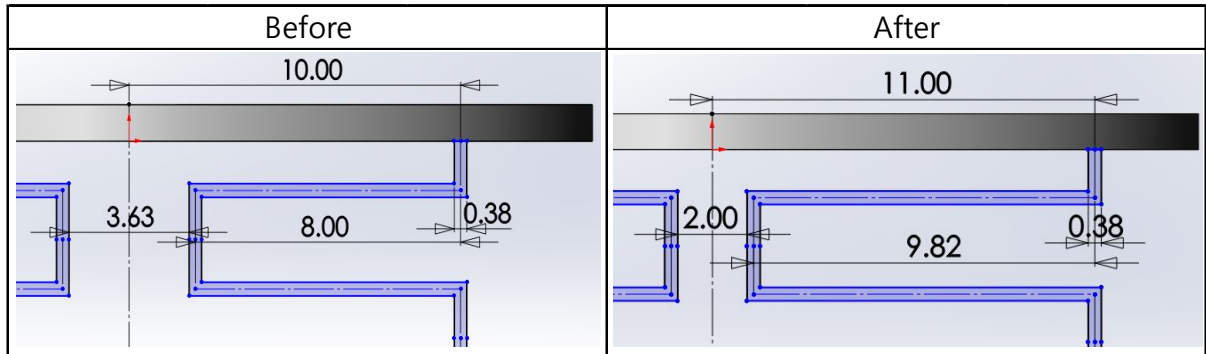


Figure 24. Spring design modification.

The modified spring models then go through simulations with the same settings as Chapter 3 to simulate the maximum stresses and spring constants. The modified spring design is expected to improve the spring performance.

### 3.4 Modification results

The folded and curved spring models was simulated with the same setting as Chapter 3. The z direction is the only displacement that can be made with zero displacements in the x and y direction. The z direction displacement, 1 mm to compress the spring was simulated to calculate the maximum stress and spring constant. The tables of the maximum stress and the spring constant for the modified folded and curved designs are shown below.

Table 9. Maximum stress of modified folded spring design.

Maximum Stress (N/m <sup>2</sup> ) - 1mm movement										
Thickness # of Fold	0.250	0.375	0.500	0.625	0.750	0.875	1.000	1.125	1.250	1.500
1	1.96E+06	2.94E+06	3.98E+06	4.88E+06	5.85E+06	6.84E+06	7.87E+06	9.06E+06	9.91E+06	1.21E+07
1.5	1.99E+06	2.86E+06	3.77E+06	4.70E+06	5.62E+06	6.59E+06	7.58E+06	8.71E+06	9.67E+06	1.21E+07
2	1.80E+06	2.54E+06	3.39E+06	4.23E+06	5.13E+06	6.00E+06	6.91E+06	7.86E+06	8.72E+06	1.11E+07
2.5	1.67E+06	2.46E+06	3.22E+06	4.03E+06	4.85E+06	5.69E+06	6.62E+06	7.64E+06	8.39E+06	1.07E+07
3	1.71E+06	2.27E+06	3.00E+06	3.72E+06	4.42E+06	5.16E+06	6.26E+06	7.26E+06	7.85E+06	9.87E+06
3.5	1.61E+06	2.14E+06	2.80E+06	3.48E+06	4.29E+06	4.94E+06	6.02E+06	7.14E+06	7.46E+06	9.90E+06
4	1.51E+06	1.94E+06	2.75E+06	3.32E+06	3.90E+06	4.80E+06	5.69E+06	6.70E+06	6.59E+06	9.06E+06
4.5	1.45E+06	1.92E+06	2.36E+06	3.08E+06	3.77E+06	4.43E+06	5.03E+06	5.89E+06	6.52E+06	9.07E+06
5	1.31E+06	1.96E+06	2.35E+06	2.95E+06	3.68E+06	4.14E+06	6.36E+06	5.45E+06	6.45E+06	8.72E+06

Table 10. Spring constants of modified folded spring design.

Spring Costant (N/mm)										
Thickness # of Fold	0.250	0.375	0.500	0.625	0.750	0.875	1.000	1.125	1.250	1.500
1	0.115	0.385	0.903	1.760	3.070	4.920	7.430	10.700	14.800	26.000
1.5	0.112	0.369	0.864	1.680	2.900	4.650	7.020	10.200	14.100	24.900
2	0.106	0.355	0.815	1.580	2.730	4.390	6.660	9.640	13.100	23.500
2.5	0.101	0.336	0.777	1.500	2.600	4.160	6.310	9.160	12.500	22.500
3	0.098	0.323	0.727	1.400	2.430	3.910	5.980	8.730	12.000	21.600
3.5	0.093	0.311	0.700	1.350	2.340	3.750	5.710	8.330	11.300	21.100
4	0.089	0.289	0.667	1.284	2.219	3.563	5.399	7.893	11.010	20.440
4.5	0.088	0.287	0.658	1.205	2.091	3.387	5.182	7.451	10.574	19.506
5	0.079	0.260	0.611	1.198	2.066	3.221	4.938	7.261	9.850	18.568

Table 11. Maximum stress of modified curved spring design.

Maximum Stress (N/m <sup>2</sup> ) - 1mm movement										
Thickness # of Curve	0.250	0.375	0.500	0.625	0.750	0.875	1.000	1.125	1.250	1.500
1										
1.5	4.19E+06	5.06E+06	6.06E+06	7.55E+06	8.86E+06	1.02E+07	1.16E+07	1.32E+07	1.52E+07	1.93E+07
2	3.89E+06	4.00E+06	5.20E+06	6.22E+06	7.17E+06	8.16E+06	9.44E+06	1.07E+07	1.25E+07	1.63E+07
2.5	3.34E+06	4.27E+06	4.85E+06	5.67E+06	6.58E+06	8.36E+06	8.62E+06	9.86E+06	1.12E+07	1.51E+07
3	3.24E+06	3.66E+06	5.03E+06	4.88E+06	6.10E+06	6.57E+06	7.83E+06	8.76E+06	1.04E+07	1.44E+07
3.5	3.24E+06	4.19E+06	5.81E+06	5.35E+06	5.11E+06	6.13E+06	7.17E+06	8.24E+06	1.10E+07	1.39E+07
4	2.51E+06	3.50E+06	4.27E+06	4.26E+06	4.91E+06	6.21E+06	6.75E+06	6.89E+06	1.20E+07	1.42E+07
4.5	2.72E+06	3.26E+06	3.60E+06	4.10E+06	4.33E+06	4.76E+06	6.78E+06	7.32E+06	9.05E+06	1.13E+07
5	1.94E+06	2.71E+06	3.09E+06	3.81E+06	4.24E+06	4.98E+06	5.81E+06	6.60E+06	8.32E+06	1.12E+07

Table 12. Spring constants of modified curved spring design.

Spring Costant (N/mm)										
Thickness # of Curve	0.250	0.375	0.500	0.625	0.750	0.875	1.000	1.125	1.250	1.500
1										
1.5	0.198	0.572	1.318	2.572	4.481	7.178	10.820	15.576	21.676	39.243
2	0.179	0.494	1.152	2.205	3.825	6.127	9.262	13.345	18.584	33.298
2.5	0.193	0.465	1.014	1.946	3.389	5.466	8.181	11.810	16.480	29.755
3	0.222	0.447	0.930	1.757	3.049	4.893	7.432	10.768	15.035	26.713
3.5	0.203	0.469	0.906	1.635	2.769	4.475	6.822	9.878	15.834	26.363
4	0.172	0.421	0.770	1.476	2.852	4.309	6.394	9.183	13.042	22.939
4.5	0.135	0.611	0.988	1.561	2.488	3.880	5.875	8.549	11.965	22.394
5	0.179	0.467	0.799	1.354	2.253	3.600	5.500	7.959	11.209	19.650

From the result, clear observation is made that modifications at the spring design lower the maximum stress and spring constant at some level. The folded design models have lower values in maximum stress and spring constant in general as simulations in Chapter 3 showed before. The improvement in spring performance is calculated by comparing the maximum stresses and the spring constants before and after the modification and calculating the average percentage in difference between values. Table 13 indicates the decrease of these measurements by the model modification in percentage values.

Table 13. Change from modification in percentage.

Change from modification (%)			
	Folded	Curved	Average
Maximum Stress	22.08%	26.69%	24.39%
Spring Constant	35.30%	38.77%	37.03%

In both designs, the maximum stress reduced less than the spring constant. In other words, extending the length of a spring is effective on reducing the spring constant. This was expected since the bending stress depends less than the spring constant does on the length of the beam according to the beam deflection theory. The decreased amounts of both measurements in percentage are higher for curved design. However, the actual values of the maximum stress and the spring constant are lower in the folded design. Modification in design is effective since on average we have 24.39% decrease in maximum stress and 37.03% in spring constant with the same spring wall thickness.

Stress distribution follows the trend equal to the previous simulations. The spring models with the folded design have the maximum stress exerted on either inside or outside the vertical wall where the bending occurs except for .250 mm thickness where they have the maximum stress at the horizontal edge of the fold due to their low thickness profile. The spring model with the curved design have a stable stress distribution trend where they have the maximum stress only at the inner wall of the curvature. Although the maximum stress is high in value, the curved spring model has more uniform and predictable characteristic in stress distribution.

Table 14. Average change in maximum stress and spring constant by number of folds.

Change in Maximum Stress By Number of Fold										
Thickness	0.250	0.375	0.500	0.625	0.750	0.875	1.000	1.125	1.250	1.500
Avg(per 0.5 fold)	-8.163E+04	-1.219E+05	-2.046E+05	-2.415E+05	-2.711E+05	-3.375E+05	-1.891E+05	-4.504E+05	-4.323E+05	-4.213E+05
Change in Spring Constant By Number of Fold										
Thickness	0.250	0.375	0.500	0.625	0.750	0.875	1.000	1.125	1.250	1.500
Avg(per 0.5 fold)	-0.005	-0.016	-0.036	-0.070	-0.125	-0.212	-0.311	-0.430	-0.619	-0.929

Table 14 represents the average change in maximum stress and spring constant per 0.5-fold for different thickness values. The negative values in the table mean the average values are decreased as the number of folds is increases by 0.5-fold. As the thickness increases, the impact of the number of folds increases, bringing higher change of maximum stress and spring constant.

Table 15. Average change in max. stress and spring constant by thickness in folded spring.

Change in Maximum Stress By Thickness		Change in Spring Constant By Thickness	
Number of Fold	Avg(per .125mm)	Number of Fold	Avg(per .125mm)
1	9.931E+05	1	1.836
1.5	9.599E+05	1.5	1.749
2	8.644E+05	2	1.624
2.5	8.404E+05	2.5	1.550
3	7.673E+05	3	1.488
3.5	7.305E+05	3.5	1.401
4	6.350E+05	4	1.365
4.5	6.336E+05	4.5	1.311
5	6.425E+05	5	1.221

Table 15 shows the average change in maximum stress and spring constant per 0.125 mm thickness change for various numbers of folds. The positive numbers indicate that with the same fold number, the maximum stress or the spring constant increase in average value when the



thickness is increased by 0.125 mm. With fewer numbers of folds, the thickness change brings dramatic change of the maximum stress and the spring constant with highest number. As the number of folds increases, the impact of thickness gets lower.

Table 16. Average change in maximum stress and spring constant by number of curves.

Change in Maximum Stress By Number of Curve										
Thickness (mm)	0.250	0.375	0.500	0.625	0.750	0.875	1.000	1.125	1.250	1.500
Avg(per 0.5 curve)	-3.216E+05	-3.356E+05	-4.237E+05	-5.349E+05	-6.601E+05	-7.460E+05	-8.300E+05	-9.453E+05	-9.770E+05	-1.157E+06
Change in Spring Constant By Number of Curve										
Thickness (mm)	0.250	0.375	0.500	0.625	0.750	0.875	1.000	1.125	1.250	1.500
Avg(per 0.5 curve)	-0.003	-0.015	-0.074	-0.174	-0.318	-0.511	-0.760	-1.088	-1.495	-2.799

The curved spring models have the similar trend in average change of maximum stress and spring constant. As the thickness increases, the average decrement in values get larger also. However, from the thickness of 0.500 mm, the average maximum stress and spring constant change are much larger in value than those of the folded models. In the curved spring model, the impact of added half fold on stress and spring constant grows up much rapidly than in folded spring model cases.

Table 17. Average change in max. stress and spring constant by thickness in curved spring.

Change in Maximum Stress By Thickness		Change in Spring Constant By Thickness	
Number of Curve	Avg(per .125mm)	Number of Curve	Avg(per .125mm)
1		1	
1.5	1.372E+06	1.5	2.685
2	1.071E+06	2	2.301
2.5	9.811E+05	2.5	2.036
3	8.915E+05	3	1.852
3.5	9.703E+05	3.5	1.954
4	1.181E+06	4	1.609
4.5	7.911E+05	4.5	1.479
5	7.983E+05	5	1.379

The spring models with the same number of curves have average change in maximum stress and spring constant as Table 17. With fewer number of curves, the thickness change brings dramatic change in maximum stress and spring constant. As the number of curve increases, the impact of thickness gets lower. The values of average change in stress and spring constant are higher with the curved design than the folded design which means the thickness has higher influence on stress and spring constant.

## **CHAPTER 4**

### **EXPERIMENT AND RESULTS**

For the daily necessities' dispenser, including shampoo, soap and lotion, spring in the pump mechanism performs the core function in the pumping action. The two main properties that are most important in designing the spring in the pump mechanism, are a spring constant which indicates the relationship between the activation pressure and compression of pump to release the contents, and the life cycle which explains how long you can use that product. In the previous chapters of theoretical approach and simulation, we developed the plastic spring design by using theoretical calculation of spring constants and performing simulation on designs to compare the spring constant and the maximum stress in the design. From the simulation section, a high number of fold or curve had advantage on distributing the stress. Before selecting the models for 3D printing, 5 sample soap, lotion, and shampoo pump dispensers are tested for their spring constants and get the resulting spring constants from 0.108 N/mm to 1.538 N/mm. We used this range of spring constant to select the models, based on their spring constants from Table 10 and Table 12 from Chapter 3. For the experiment, 4 models are selected each from folds and curves with high numbers of spring structure which are 4 and 5, and the thickness of 0.500 mm and 0.750 mm based on their theoretical and simulation results of spring constants. In this section, total of 8 models which have different spring base unit design, thickness, and number of spring structure will go under two experiments to test the spring constant and life cycle of the spring models.

#### 4.1 Spring constant test

Eight models selected for experiment, were printed from 3D printer and we tested their spring constants. As the spring constant is the value of force needed to compress a spring in unit length, the spring models were pressed to a given length to figure out the force needed. Figure 25 shows setting for the spring constant testing.

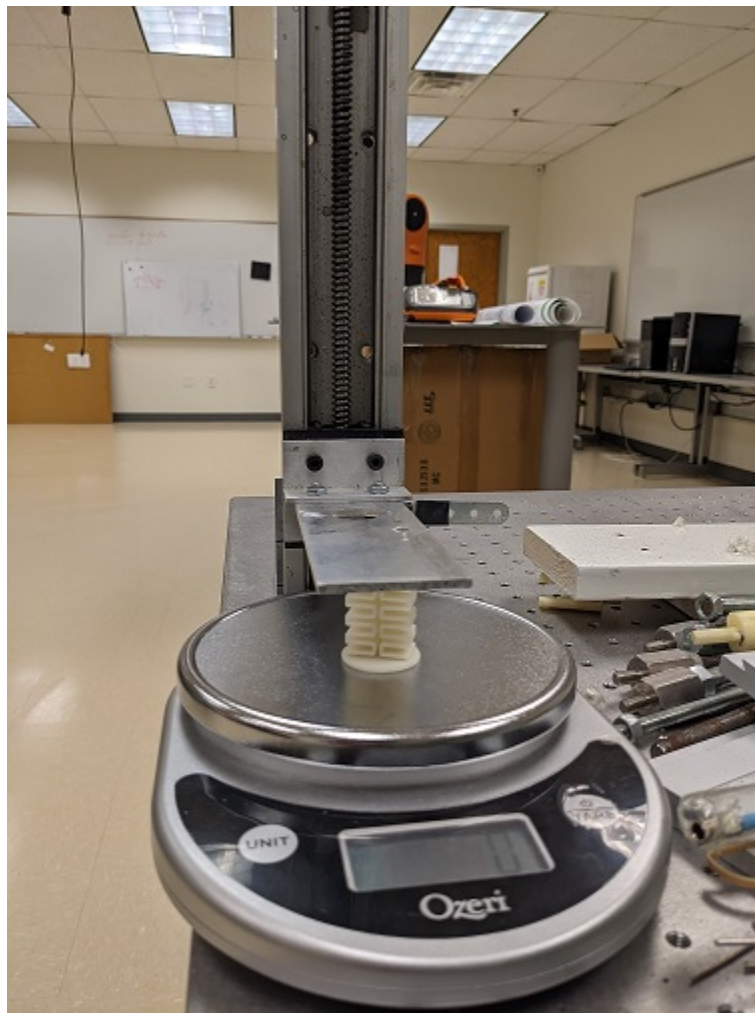


Figure 25. Spring constant test setup.

Precision balance is tared to set the weight to 0 with the plastic spring on it, and then the linear motion system pressed the plastic spring to certain a distance to figure out how much weight has been applied at the balance to calculate the spring constant. The linear motion system in this experiment is MS33-10021 from Thompson, and has 0.125 inch which is 3.175 mm travel length per shaft revolution [25]. In the experiment, three different travel lengths which are 0.5, 1.0, and 1.5 revolution of compression was applied to each plastic spring models to record the weight applied on the balance and then, the average spring constant value converted into N/mm to be compared to the theoretical and simulation spring constants. All weight values were measured 10 times and averaged to minimize any error in the experiment. Figure 26 shows the gram-force result of different travel lengths for 4.0-fold, 0.750mm folded spring model. The slope of gram-force to travel length is taken for the spring constant in this case, 1.629 N/mm. Same method applied to measure spring constants of eight models in the experiment. Table 18 and 19 show the results of spring constants from theory, simulation and experiment.

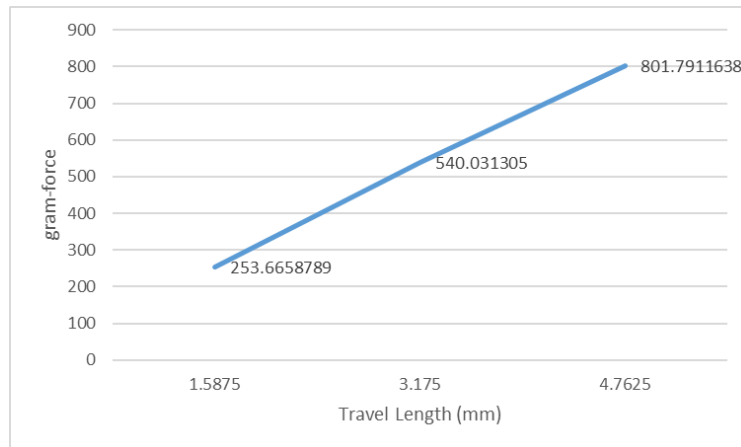


Figure 26. Gram-force of 4.0-fold, 0.750 mm folded spring model with different travel lengths

Table 18. Spring constants from theory, simulation, and experiment for folded spring design.

Theory			Simulation			Experiment		
Spring Constant (N/mm)								
Thickness # of Fold	0.500	0.750	Thickness # of Fold	0.500	0.750	Thickness # of Fold	0.500	0.750
4	0.463	1.614	4	0.667	2.219	4	1.210	1.629
5	0.413	1.439	5	0.611	2.066	5	1.117	1.632

Table 19. Spring constants from theory, simulation, and experiment for curved spring design.

Simulation			Experiment		
Spring Constant (N/mm)					
Thickness # of Curve	0.500	0.750	Thickness # of Curve	0.500	0.750
4	0.770	2.852	4	1.279	2.317
5	0.799	2.253	5	1.248	2.213

For the folded models with 0.500 mm thickness, the spring constants are higher in simulation and experiment than the spring constant from theory. However, for 0.750 mm thickness models, the spring constants from experiment are smaller than simulation and similar to theoretical values. In theoretical calculation, small values, including the deflection due to the compression, are ignored to simplify the calculation. The ignored values and the design how we build the spring models with two spring structures and two plates in top and bottom can lead us to the difference in spring constants from theoretical calculation and simulation. In prototyping of spring models, there are many settings and properties that can affect the properties of the final models. The 3D printer's settings such as the printing density, the direction of printing, and the printing resolution can change the properties of a printed model. In addition, the ABS plastic used for printing also can have different properties compared to what we used in theoretical

approach and simulation. 0.500 mm models from 3D printer have higher spring constants than simulation and show stiffer characteristic than expected. However, 0.750 mm models have lower spring constants than simulation and show soft characteristic than expected. As mentioned above, this randomness comes from settings and actual printing. However, the printed models still show the similar basic trend of spring constants to the theoretical and simulation result. When the model got more folds, the spring constant decreased, and when the model got thicker, the spring constant increased.

The curved spring models showed the same trend as the folded spring model. The curved model does not have theoretical spring constant since it is not practical to apply the beam bending theory to highly curve structure. Comparing the simulation and experiment results, the similar trend can be observed compared to the folded models. For the 0.500 mm thickness model, the spring constants are higher in experiment but for the 0.750 mm model, spring constants are lower in experiment compared to the simulation. The relationship between thickness, number of curves and spring constants still remain the same in the experiment.

## **4.2 Durability test**

Industrial springs normally have industry standard for its life cycle about 10,000 to 15,000 uses or a spring life of about 5 years on average [26]. If a spring design does not reflect the usage efficiently, and more force is applied than what the spring was designed to handle, breakage can occur and shorten the life cycle. A spring needs to be designed according to its usage, and needs to have enough life cycle in that usage. In addition, repeating compression should not affect the

spring constant unless it reaches its life cycle. In this test, eight models are going under a repeated compression by a DC motor and a small disc attached on the motor. The maximum compression distance for the spring is 18 mm. The spring constant is remeasured after 500 compressions. Figure 27 shows the setting of the test. Tables 20 and 21 show the measurement results for the folded and curved models, respectively. We conclude that the 500 repeated compressions did not dramatically change the spring constants of the both designs.

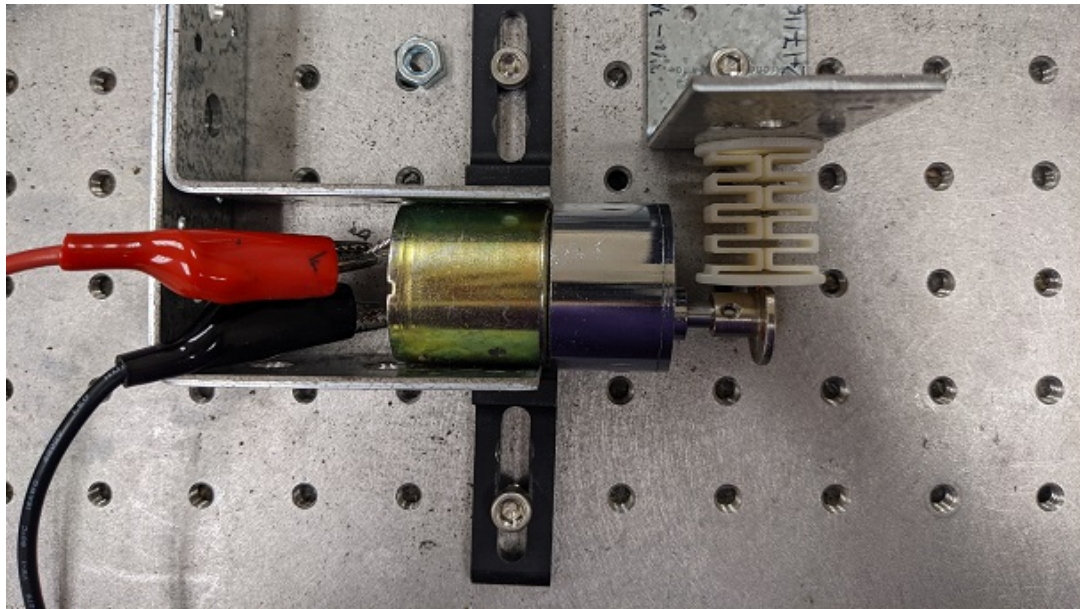


Figure 27. Durability test setup



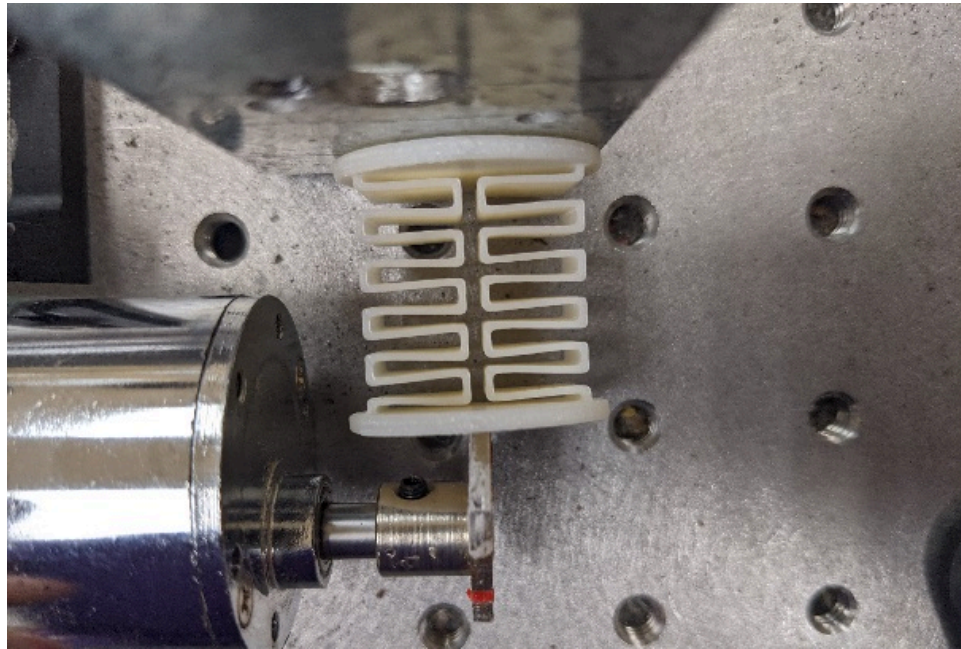


Figure 28. Spring compressed in durability test

Table 20. Spring constants before, and after the repetition test for folded spring models.

Before			After		
Spring Constant (N/mm)					
Thickness # of Fold	0.500	0.750	Thickness # of Fold	0.500	0.750
4	1.210	1.629	4	1.210	1.751
5	1.117	1.632	5	1.114	1.573

Table 21. Spring constants before, and after the repetition test for curved spring models.

Before			After		
Spring Constant (N/mm)					
Thickness # of Curve	0.500	0.750	Thickness # of Curve	0.500	0.750
4	1.279	2.317	4	1.510	2.241
5	1.248	2.213	5	1.311	2.210

With these observations, our models have longer life cycle than 500 uses. Since they are made of plastic, the models might have shorter life cycle than metallic springs, but this can be improved by how springs are designed and what materials are used for the springs. More importantly, since average amount from one pumping from daily necessities such as soap pumps is 2.0 ml, we can assume that 500 uses are enough for each pump.

## CHAPTER 5

### SUMMARY AND FUTURE WORK

In this paper, we developed a design for a new plastic spring to resolve a recycling issue in daily necessities including dispenser pump-mechanisms for soap and shampoo. This problem is important because plastic is one of the major wastes in the world, and still people are using a lot of plastic products which cannot be recycled or is hard to recycle. We proposed a way to design a spring structure made from ABS plastic that can replace the metallic spring in pump mechanism of daily necessities for efficient recycling of the pump mechanism. The new spring structure uses compliant mechanisms for elastic movement for compression. We tested the new spring structure design in theoretical calculation, simulation and experiment with actual spring model. Although there were uncertainties that affect the spring stiffness depending on testing methodologies, we found a clear effect of thickness and the number of layers of spring structures on spring stiffness. Through this research, we provided various numerical results for stiffness and maximum stress of the models depending on the thickness and the number of layers of spring structures. These results are expected to suggest a way to select the model for desired spring stiffness that can satisfy needs from different applications.

Future work includes the application of the plastic spring for an MRI-guided puncture robot which works in high magnetic field. Percutaneous needle puncture operation uses a needle to set up a channel to the target tissue location in the human body, and the physician completes diagnosis and treatment through this channel [27]. For MRI-guided needle puncture robot, the strong magnetic field limits the use of devices containing ferromagnetic materials like traditional motors or metallic springs. In [27], pneumatic working principle is implemented to replace the

traditional components for required movements and applications, but plastic spring in this paper has potential to be utilized in this application. Since the plastic spring can be designed in any size, for any desired spring stiffness customized to the purpose, it has flexibility to be utilized in many applications. That means plastic spring can be designed in extremely small size to applied in extremely small application with desired stiffness by customized design. Pneumatic cylinders in the MRI-guided puncture robot can be replaced by plastic springs or cylinders and spring can be utilized together to store, and release the energy in higher precision for desired performance. With the spring attached to the needle with pneumatic cylinder, puncture of the needle can be easily controlled for more precise prick and retraction.

## REFERENCES

- [1] "Current World Population," Worldometer. [Online]. Available: <https://www.worldometers.info/world-population/>.
- [2] K. van Lohuizen, "Drowning in garbage," The Washington Post, 21-Nov-2017. [Online]. Available: <https://www.washingtonpost.com/graphics/2017/world/global-waste/>.
- [3] C. L. Guern, "When The Mermaids Cry: The Great Plastic Tide," Plastic Pollution, Nov-2019. [Online]. Available: <https://plastic-pollution.org/>.
- [4] Ellen MacArthur Foundation, "The New Plastics Economy Rethinking the future of plastics" presented at the World Economic Forum., Davos-Klosters, Switzerland, 2016
- [5] L. Parker, "Eight Million Tons of Plastic Dumped in Ocean Every Year," New Study Shows Plastic in Oceans Is on the Rise, 10-Oct-2017. [Online]. Available: <https://www.nationalgeographic.com/news/2015/2/150212-ocean-debris-plastic-garbage-patches-science/>.
- [6] M. T. Brown and V. Buranakarn, "Emergy indices and ratios for sustainable material cycles and recycle options," Resources, Conservation and Recycling, vol. 38, no. 1, pp. 1–22, Apr. 2003.
- [7] E. Macarthur, "Beyond plastic waste," Science, vol. 358, no. 6365, pp. 843–843, Nov. 2017.
- [8] A. Monaghan, "Which items can't be recycled?," 16-Mar-2018. [Online]. Available: <https://www.theguardian.com/environment/2018/mar/16/which-items-cant-be-recycled-plastic-bags-coffee-cups>.
- [9] J. Wray, "How to recycle just about anything," Cosmetics Business, 11-Sep-2020. [Online]. Available: [https://www.cosmeticsbusiness.com/news/article\\_page/How\\_to\\_recycle\\_just\\_about\\_anything/169630](https://www.cosmeticsbusiness.com/news/article_page/How_to_recycle_just_about_anything/169630).
- [10] S. K. Vishwakarma, P. Pandey, and N. K. Gupta, "Characterization of ABS Material: A Review," Journal of Research in Mechanical Engineering, vol. 3, no. 5, pp. 13–16, Apr. 2017.
- [11] Lipson, H., Moon, F. C., Hai, J., and Paventi, C. 17-Oct-2004. "3-D Printing the History of Mechanisms." ASME. J. Mech. Des. September 2005; 127(5): 1029–1033.
- [12] L. L. Howell, Compliant mechanisms. New York, NY: John Wiley & Sons, 2011.

- [13] L. L. Howell, S. P. Magleby, and B. M. Olsen, Handbook of compliant mechanisms. Chichester, UK: Wiley, 2013.
- [14] D. Drummer, S. Cifuentes-Cuéllar, and D. Rietzel, “Suitability of PLA/TCP for fused deposition modeling,” Rapid Prototyping Journal, vol. 18, no. 6, pp. 500–507, 2012.
- [15] G. Rouilloux, “Read @Kearney: Plastics. The future for automakers and chemical companies,” Kearney. [Online]. Available: <https://www.de.kearney.com/chemicals/article?%2Fa%2Fplastics-the-future-for-automakers-and-chemical-companies>.
- [16] A. L. Andrady and M. A. Neal, “Applications and societal benefits of plastics,” Philosophical Transactions of the Royal Society B: Biological Sciences, vol. 364, no. 1526, pp. 1977–1984, Jul. 2009.
- [17] L. L. Howell and A. Midha, “A Loop-Closure Theory for the Analysis and Synthesis of Compliant Mechanisms,” Journal of Mechanical Design, vol. 118, no. 1, pp. 121–125, Mar. 1996.
- [18] A. Midha, Y. Annamalai, S. K. Kolachalam, S. G. Bapat, and A. B. Koli, “On a Compliant Mechanism Design Methodology Using the Synthesis with Compliance Approach for Coupled and Uncoupled Systems,” Advances in Mechanisms, Robotics and Design Education and Research Mechanisms and Machine Science, pp. 95–116, 2013.
- [19] J. Hopewell, R. Dvorak, and E. Kosior, “Plastics recycling: challenges and opportunities,” Philosophical Transactions of the Royal Society B: Biological Sciences, vol. 364, no. 1526, pp. 2115–2126, Jul. 2009.
- [20] T. J. Lardner, An introduction to the mechanics of solids. With SI units. 2.ed. New York, NY: McGraw-Hill, 1978.
- [21] Carol Livermore, course materials for 6.777J / 2.372J Design and Fabrication of Microelectromechanical Devices, Spring 2007. MIT OpenCourseWare(<http://ocw.mit.edu/>), Massachusetts Institute of Technology. Downloaded on 12 Apr 2020.
- [22] R. K. Bhattacharjya, “Area Moments of Inertia,” in ME 101: Engineering Mechanics, 2020.
- [23] Dielectric Manufacturing, “Material Properties of ABS - Acrylonitrile-Butadiene-Styrene,” Dielectric Manufacturing, 24-Mar-2020. [Online]. Available: <https://dielectricmfg.com/knowledge-base/abs/>.
- [24] A. Bertram and Glüge Rainer, Solid mechanics: theory, modeling, and problems. Cham: Springer, 2015.

[25] Linear Motion Systems. Thomson, Radford, VA, 2018.

[26] 2017 September 29, “Typical Lifespan of Stainless Steel Springs: Coil Spring Design,” Typical Lifespan of Stainless Steel Springs | Coil Spring Design, 23-May-2019. [Online]. Available: <https://www.jamesspring.com/news/how-long-do-springs-last-answers-to-your-questions/>.

[27] B. Zhao, Y. Fu, Y. Yang, P. Zhang, and Y. Hu, “Design and control of a MRI-compatible pneumatic needle puncture robot,” *Computer Assisted Surgery*, vol. 24, no. sup2, pp. 87–93, 2019.

[28] D. Ford, “COVID-19 Has Worsened the Ocean Plastic Pollution Problem,” *Scientific American*, 17-Aug-2020. [Online]. Available: <https://www.scientificamerican.com/article/covid-19-has-worsened-the-ocean-plastic-pollution-problem/>.

## **BIOGRAPHICAL SKETCH**

Sungju Park received his Bachelor of Science in Mechanical Engineering from Georgia Institute of Technology in Atlanta, Georgia. He spent three years in Kumho Tire Georgia plant as a mechanical engineer for maintenance and machinery team. In August of 2018, he joined the graduate program in mechanical engineering at The University of Texas at Dallas. In January of 2019, he became a teaching assistant and started his research under the supervision of Dr. Wooram Park.



# **CURRICULUM VITAE**

## **PERSONAL DETAILS**

Name: Sungju Park

Email: [sxp170038@utdallas.edu](mailto:sxp170038@utdallas.edu)

## **EDUCATION**

2005-2009: Matignon High School

2009-2015: Georgia Institute of Technology

2018-2020: University of Texas at Dallas

## **PROFESSIONAL EXPERIENCE**

2015-2018: Kumho Tire Georgia | Mechanical Engineer

## **TEACHING/RESEARCH ASSISTANT EXPERIENCE**

2019-2020: Teaching Assistant (MECH 3350: Kinematics and Dynamics of Mechanical Systems)

## **PUBLICATIONS**

- Park, S., Sugumar, V. P., Michael, V. L. (2019). Modeling and Simulation of a Collision Avoidance System.
- Park, S., Whitworth, C., Javadzadeh, P., (2019). Optimizing the Profit of a Medium Scale Home Aquaponics System.

## **TECHNICAL SKILLS**

3D Modeling, Simulation, FEA, Project Management, Data Analysis

## **LANGUAGES**

English, Korea, Japanese